Materials Advances

ROYAL SOCIETY OF CHEMISTRY

REVIEW

View Article Online
View Journal | View Issue

Cite this: *Mater. Adv.*, 2024, 5, 4563

Unveiling the future of steel corrosion inhibition: a revolutionary sustainable odyssey with a special emphasis on N^+-containing ionic liquids through cutting-edge innovations

Sanjukta Zamindar, [ab] Sukdeb Mandal, [ab] Manilal Murmu [c] and Priyabrata Banerjee *[ab]

Received 16th February 2024,
Accepted 26th April 2024

DOI: 10.1039/d4ma00156g

rsc.li/materials-advances

The advancement of sustainable and green technologies for the mitigation of corrosion, driven by the escalating awareness of ecological considerations and stringent environmental regulations, is of paramount importance. Over the past decade, significant attention has been directed towards inhibiting metallic corrosion using ionic liquids (ILs) owing to their intriguing characteristic properties and their capacity to be adsorbed, followed by the formation of an effective barrier film onto metallic surfaces. This review comprehensively explores the application of ILs with a special emphasis on N^+-containing ILs as "next-generation corrosion inhibitors" for metal substrates, specifically steel surfaces, across various aggressive environments, highlighting the trend towards "hype *vs.* hope". Additionally, this review elucidates the adsorption mechanism and intriguing factors that trigger the adsorption process of ILs by employing state-of-the-art experimental as well as computational approaches to gain a comprehensive understanding of their corrosion inhibition potential.

[a] *Electric Mobility and Tribology Research Group, CSIR-Central Mechanical Engineering Research Institute, Mahatma Gandhi Avenue, Durgapur 713209, West Bengal, India. E-mail: pr_banerjee@cmeri.res.in*
[b] *Academy of Scientific and Innovative Research (AcSIR), Ghaziabad 201002, Uttar Pradesh, India*
[c] *Department of Nuclear and Quantum Engineering, Korea Advanced Institute of Science and Technology, Daejeon 34141, South Korea*

1. Introduction

Corrosion is an inevitable process that involves the irreversible degradation of metals or alloys through chemical or electrochemical reactions with their surroundings. Corrosion causes severe destruction of metallic resources, resulting in health

Sanjukta Zamindar

Sanjukta Zamindar received her bachelor's degree in Chemistry from Bankura Christian College under The University of Burdwan, Burdwan, India. She received her master's degree in chemistry from The University of Burdwan, Burdwan, India. Currently, she is pursuing PhD in Chemical Sciences as a Junior Research Fellow at CSIR-Central Mechanical Engineering Research Institute (CMERI), Durgapur, affiliated to Academy of Scientific and Innovative Research (AcSIR) under the supervision of Dr Priyabrata Banerjee. Her research mostly focuses on the development of novel organic corrosion inhibitors as well as smart anticorrosive coating materials for the protection of metallic substrates against adverse environments.

Sukdeb Mandal

Sukdeb Mandal received his bachelor's degree in chemistry from the Bankura Christian College under the University of Burdwan, Burdwan, India. He obtained his MSc degree in Chemistry from Visva Bharati University, Santiniketan, India. Currently, he is pursuing PhD in Chemistry from Academy of Scientific and Innovative Research (AcSIR) under the supervision of Dr Priyabrata Banerjee. His current research interests include the development of organic as well as metal–organic functional materials as next-generation corrosion inhibitors and lubricant additives.

hazards and/or loss of flora and fauna, including mankind, along with huge economic impacts across the world.[1–5] Its pervasive impact affects the economic growth trajectories of both developed and developing nations. According to a study conducted by the National Association of Corrosion Engineers (NACE), the United States experiences an economic loss that is roughly equivalent to 3.1% of the country's Gross Domestic Product (GDP) due to corrosion.[6,7]

Metal and their alloys find widespread industrial usage, such as manufacturing, architecture, transportation, and oil refineries, but their ensuing corrosion due to the adverse environments has become an alarming issue.[8,9] Steel, being an affordable and robust material, is one of the most widely utilised go-to building materials globally and is used in several infrastructures, buildings, vehicles, machinery, and other applications. Among the other construction materials, it offers the best strength-to-weight ratio and is fully recyclable. Large construction projects, mainly those constructed of steel, require a long life span of infrastructural materials. During this time, metallic structures are exposed to several adverse environments and many other harsh conditions that result in the deterioration of the metallic structures. Accordingly, the longevity of the metallic bodies is highly compromised. Therefore, to enhance longevity and protect such type of vital assets in terms of economic and environmental aspects, corrosion protection is highly essential. The intrinsic ability of a metal to chemically react with its surroundings is the primary factor in determining the magnitude of the ensuing loss. Elemental composition, temperature, mechanical variables, electrical potential difference, pH, and environmental circumstances are some of the factors that affect the rate of metal corrosion. Corrosion may be minimized using appropriate techniques, such as the application of potential corrosion inhibitors and protective coatings.[10–21]

In recent years, several corrosion mitigation strategies have been developed. The application of synthetic inhibitors has become the most promising approach owing to their low cost and ease of utilization in several industries. One of the most commonly used methods to combat aqueous corrosion of various metals and alloys is the application of organic compounds as inhibitors. The majority of effective inhibitors consist of an organic scaffold containing heteroatoms (nitrogen, oxygen, phosphorous, and sulphur) and unsaturation (*e.g.*, double or triple bonds) that function as active centres for donor–acceptor (D–A) type interaction with the metal atom.[3,22–26]

The molecular structure of organic molecules plays a crucial role in their ability to act as effective corrosion inhibitors. These organic molecules contain unsaturated conjugated bonds, aromatic and/or heterocyclic moieties, and polar functional groups, such as nitro ($-NO_2$), amine ($-NH_2$), hydroxyl (–OH), carboxyl (–COOH), ester (–COOR), amide ($-CONH_2$), *etc*. These functional groups enable the organic molecules to adhere to the metal substrate and form a protective layer on its surface, thereby preventing corrosion. The unsaturated conjugated bonds and aromatic and/or heterocyclic moieties further enhance the efficacy of organic molecules as corrosion inhibitors. The functional groups act as highly proficient D–A centers that strongly interact with metal atoms, effectively facilitating the adsorption of the inhibitor molecules onto the exposed metal exterior. Inhibitor molecules adsorbed on metal surfaces can hinder corrosion processes, including anodic, cathodic, or both, at the metal–electrolyte interface.[6,27–32]

Nevertheless, traditional organic inhibitors face limitations due to tedious synthetic processes, low thermal stability,

Manilal Murmu

Dr Manilal Murmu is currently a post-doctoral fellow at the Korea Advanced Institute of Science & Technology (KAIST), Daejeon, South Korea. His current research interest involves the improvement of corrosion and wear resistance of NPP cooling water components using a nanoporous compact oxide layer. He earned his MSc degree in Chemistry from Visva Bharati University, Santiniketan, India. He obtained his doctoral award from the Academy of Scientific and Innovative Research (AcSIR) under the joint supervision of Dr Priyabrata Banerjee and Dr Naresh Chandra Murmu.

Priyabrata Banerjee

Dr Priyabrata Banerjee is Senior Principal Scientist, CSIR-CMERI and Professor (AcSIR), India. Dr Banerjee is currently a Fellow of the Royal Society of Chemistry (FRSC). He received his PhD in 2007 from the Indian Association for the Cultivation of Science, Jadavpur, Kolkata, India. He did his post-doctoral research at the Max Planck Institute for Bioinorganic Chemistry, Müelheim, Germany, during 2007–2010. He was a DST-DAAD visiting fellow at the University of Water Science, HTW Dresden, Germany. He is a CSIR-Raman Research Fellow (2019–2020) at Ghent University, Belgium. He has published over 175 research papers and several review articles in reputable journals. His current research focuses on the development of corrosion inhibitors, smart anticorrosive coatings and lubricant additives along with selective detection and removal of toxic substances from waste water.

reduced chemical stability, and a gradual loss of protective efficacy over time.[33–35] Therefore, recognizing the imperative for environmentally friendly and sustainable corrosion prevention technologies has become paramount. This shift is fuelled by heightened awareness of ecological considerations and adherence to stringent environmental regulations. Over the past decade, significant attention has been directed towards inhibiting metallic corrosion using ILs owing to their intriguing characteristics, such as their low vapor pressure, non-inflammable nature, higher thermos-chemical stability, and their capability to get adsorbed onto metallic surfaces.[36] ILs are molten salts basically comprising anions and cations that have an organic molecular composition with intriguing physical–chemical characteristics.[37,38]

Furthermore, by combining the proper cation–anion pair, the physicochemical characteristics of ILs can be tailored to accomplish specific functions. Several ''tailor-made'' functional ILs can be developed for target-specific materials and functional applications due to their tunable characteristics. Consequently, ILs play a unique role in the formulation of novel functional materials because of their various scientific and technological applications, most remarkably in the protection of steel from corrosion damage. The beauty within the molecular structure of the IL helps in its quick film formation ability on the metallic surface. It has been observed that N^+-containing ILs have grabbed superior attention because of their facile synthesis, high yield, and better shielding nature towards corrosion.[39,40] Moreover, the inadequate solubility of typical organic and polymeric chemical substances in polar electrolytic media confines the application of these substances as corrosion inhibitors. This constraint is easily overcome by employing ILs because they exhibit high solubility in polar aqueous environments.[41–43]

There are several recent reports in the literature that deal with the comparative insight regarding the adsorption of ILs on metal surfaces to retard the rate of corrosion inhibitory actions.[44–46] This review thoroughly explores how N^+-based ILs can be used as ''green'' corrosion inhibitors to effectively reduce the corrosion rate of mild steel in various electrolytic environments. The mechanisms and adsorption behaviours of the most important five types of ILs based on ammonium, pyridinium, piperidinium, pyrrolidinium, and imidazolium cations are discussed. Additionally, the consideration of structural features, including chain length, heteroatom incorporation, ring structure, and π-electron moieties, influencing their ability to adhere to the mild steel surface and their subsequent protection ability in various electrolytic media are highlighted. To advance our understanding of their real-world corrosion inhibition potential, both modern experimental techniques and cutting-edge computational approaches have been comprehensively discussed. These dual investigative approaches aim to provide a nuanced and interconnected understanding of adsorption and corrosion inhibition, which ultimately contribute to the design and adaptation of more effective and easy-going corrosion prevention strategies for different environmental contexts based on green ILs.

2. Evolution of ILs in corrosion control

The evolution of ILs in corrosion inhibition represents a transformative journey in materials science, revolutionizing the way of protecting metals from corrosion.[47] Subsequent years have seen an increase in the design and synthesis of tailored ILs, marking notable advancements in the contemporary field. In the early stages of this evolution, around the turn of the century, researchers began to recognize the potential of ILs as effective corrosion inhibitors, stemming from their unique physicochemical properties. Researchers have been driven in the field of corrosion mitigation with ILs by diverse combinations of cations paired with anions, all aimed at optimizing their inhibitive performance. The focus then shifted towards understanding the intricate mechanisms underlying corrosion inhibition, including adsorption and film formation.

This deeper understanding has led to the design of ILs for enhanced efficacy in diverse corrosive environments. The evolution also witnessed an expansion beyond the laboratory, with ILs finding practical applications in specific industries, such as oil and gas, where corrosion poses significant challenges.

Continuous advancements in the contemporary field have yielded environmentally benign IL-based formulations that offer robust corrosion protection and minimize environmental impacts. The year-wise progression, as illustrated in Fig. 1, reflects a dynamic journey marked by relentless innovation and a deeper understanding of how ILs can serve as game changers to combat corrosion. The future has immense potential for further refinement and expansion of this technology, promising even more effective and sustainable solutions for corrosion inhibition across various industries. Currently, the primary obstacle facing the application of ILs as corrosion inhibitors is their cost. To overcome the cost barrier of ILs towards corrosion inhibition application, a techno-commercial study is required. Another effective and environmentally viable approach to overcome the cost barrier of ILs is the synthesis of deep eutectic solvents (DES) from the ILs. It has been reported that the production cost of DES is around 80% less than that of ILs. Commonly available DES is mainly choline-based ILs in association with urea, ethylene glycol, and diethanolamine. In the future, several other N-based ILs can be used for the production of DES for effective corrosion inhibition.

Another challenge of ILs in corrosion inhibition applications is their toxicity in some cases. ILs may be toxic in solute form for animals, including humans, in some cases. Therefore, it is highly necessary to formulate eco-friendly ILs for corrosion inhibition application.[48–50]

3. Classification of ILs

The year 1914 marked a significant turning point in the field of chemistry with the introduction of ethylammonium nitrate, $[EtNH_3][NO_3]$, the first IL to be recognized in scientific literature. This colourless to slightly yellowish liquid, with a melting point of 12 °C, indicated a new era in the field of science and engineering.[47,51,52] Nearly three decades later, in 1940, Frank

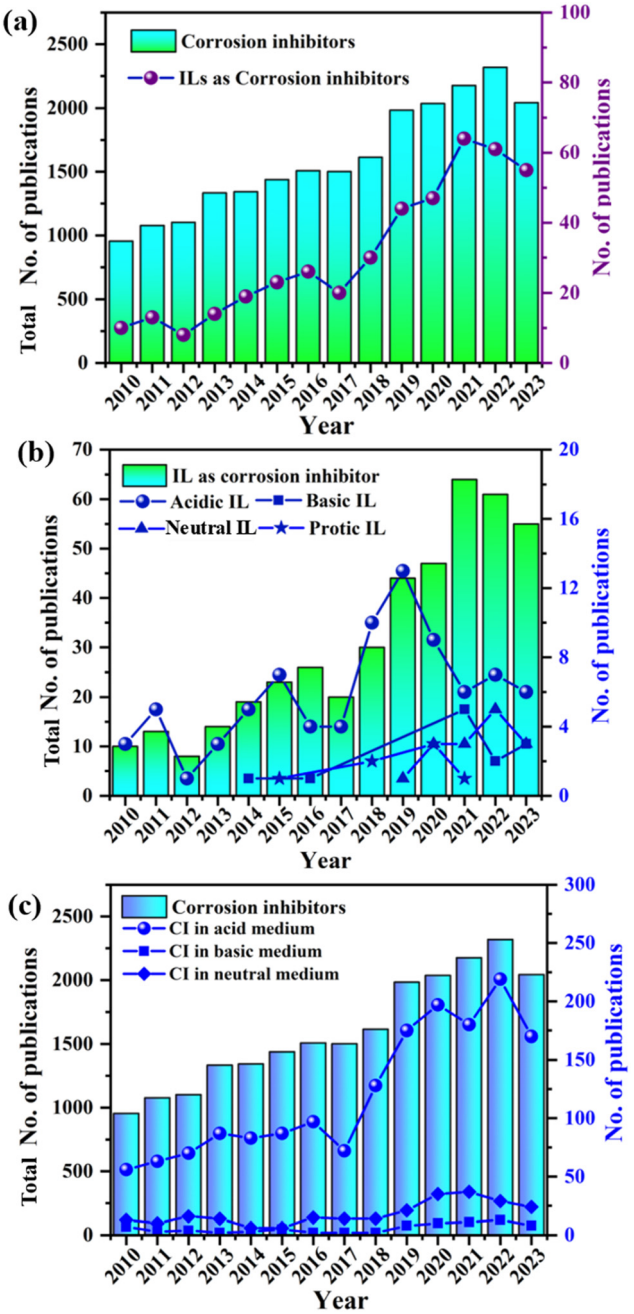

Fig. 1 Year-wise publication details about (a) the total number of corrosion inhibitors and ILs as corrosion inhibitors, (b) the number of publications of different types of ILs as corrosion inhibitors, and (c) the development of corrosion inhibitors for different aggressive mediums. Data obtained from the Scopus database (**https://www.scopus.com**) [data produced on 31st December, 2023]. Search key: acidic ionic liquid corrosion inhibitor; amphoteric ionic liquid corrosion inhibitor; basic ionic liquid corrosion inhibitor; corrosion inhibitor; corrosion inhibitor for acid medium; corrosion inhibitor for acidic medium; corrosion inhibitor for basic medium; corrosion inhibitor for neutral medium; and ionic liquid corrosion inhibitor.

Hurley and Tom Weir made another groundbreaking discovery through the development of room-temperature stable ILs. While conducting experiments with organic salts, they observed that a warm powder of alkyl pyridinium chloride, when combined with aluminium chloride, transformed into a clear, colourless liquid.[47] This remarkable observation marked the birth of a new class of materials. Despite their immense potential, ILs have remained largely overlooked for several decades, confined to the field of chemical curiosities. However, the tide began to turn in the 1970s when scientists rediscovered these intriguing liquids and their unique properties.[53–55]

Categorizing ILs into well-defined groups is a complex endeavour due to the various factors that influence their properties. These factors include the structural diversity of both cations and anions, which form the building blocks of ILs. The positively charged ions in ILs exhibit a wide structural variety, including imidazolium, pyridinium, and piperidinium-based cations.[56] Each cation type imparts distinct properties to the IL, such as melting point, viscosity, and solubility. However, the negatively charged ions also contribute significantly to the overall properties of ILs. Common anions include chloride (Cl^-), bromide (Br^-), and nitrate (NO_3^-).[56] The choice of anion can influence the IL's polarity, thermal stability, and miscibility with other solvents. ILs also have mobile ions responsible for their ionic conductivities. Moreover, these compounds have been initially categorized into several classes depending on their multi-functional properties since their invention. For instance, based on physical characteristics such as solubility, water-miscibility, viscosity, conductive nature, and the basicity or acidity of the constituent ionic species, ILs have been categorized into different groups.[57] These classes are neutral IL, acidic IL, basic IL, IL with amphoteric anions, functionalized IL, protic IL, chiral IL, supported IL, bio-IL, poly IL, and energetic IL. A categorization system was established to classify IL compounds into three generations: first-generation, second-generation, and third-generation. This classification is based on the time frame when these compounds were developed and introduced. The categorization system helps identify each generation of IL compound's characteristics and properties and their potential applications in various fields.[58] First-generation ILs contain bulky cations in their molecular structure, and they are not so stable in the presence of air and water. The evolution of second-generation ILs with the development of water/air stable IL was reported by Wilkes and Zawrotko in 1992 based on 1-ethyl-3-methylimidazolium cation and suitable anions, such as OAc^- and NO_3^-.[59] At the very beginning of the 21st century, the third-generation 'task-specific' IL was developed to overcome the drawback of the earlier developed ILs.[60–62] Additionally, another two categories of ILs, cationic IL and anionic IL, have also been found in the literature.[63] However, based on the well-established distinction between proton-donating and nonproton-donating functionality, the two most prevalent IL families are protic IL and aprotic IL.[64,65] However, this classification is also not so rigorous. Generally, ILs comprise two components, *e.g.*, the cationic and anionic parts, similar to the two glasses of a spectacle. The cationic and anionic fragments that frequently comprise ILs are presented in Fig. 2.

Accordingly, the prolonged classifications of ILs can be made based on constituent ions within its molecular scaffold.

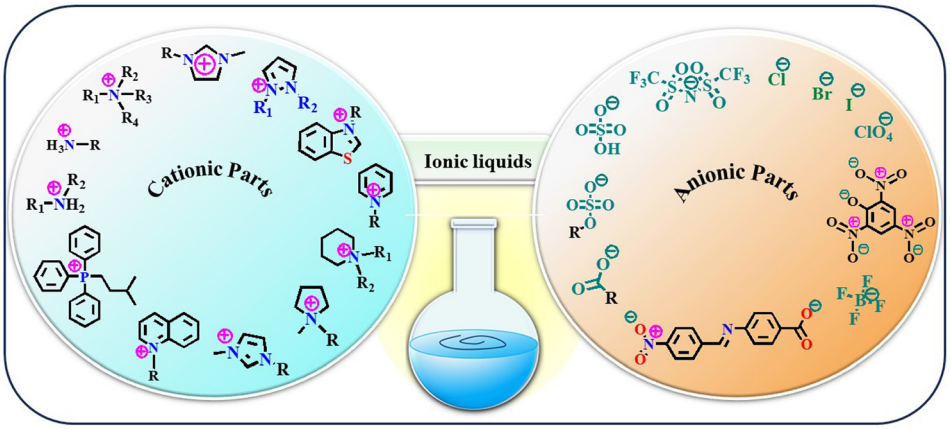

Fig. 2 Structural representation of some common cationic and anionic counterparts that combine to form ILs.

The anionic fragment may be an organic or inorganic anion such as Cl^-, Br^-, iodide (I^-), nitrate (NO_3^-) perchlorate (ClO_4^-), carboxylate ($HCOO^-$) bistriflimide ($(CF_3SO_2)_2N^-$), tetrafluoroborate (BF_4^-), and sulphate (SO_4^{2-}). The cationic component may be a derivative of ammonium, imidazolium, pyrazolium, pyrrolidinium, phosphonium, thiazolium, piperidinium, pyridinium, *etc.*, with variable substituents such as alkyl groups or aromatic rings.

4. Traits and implementations of ILs

However, ILs are a fascinating class of compounds that have captivated the scientific community with their remarkable properties. Unlike traditional salts, such as sodium chloride (NaCl) or potassium chloride (KCl), which exist as crystalline solids at room temperature, ILs are liquids comprising constituent ions. This difference arises from the asymmetrical and bulky nature of the constituent ions in ILs, which weaken ionic interactions and lowers the melting point significantly.[55,66–68] Fig. 3 represents a pictorial depiction of several intriguing properties of ILs.

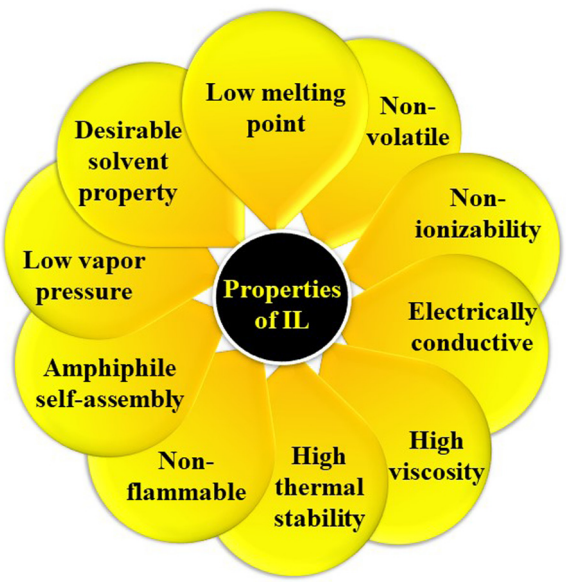

Fig. 3 Pictorial representation of the general intriguing properties of ILs.

One of the most intriguing aspects of ILs is their tunability. By carefully designing the combination of cations and anions, scientists can tailor the physical characteristics of ILs, including their viscosity, density, thermal stability, melting point, and boiling point. This allows for the creation of ILs with specific properties that are ideal for various applications.[36,37,69–72]

Furthermore, ILs possess a diverse range of other remarkable properties, such as

(i) Low vapour pressure: ILs are essentially non-volatile, making them environmentally friendly and safe to handle.[73]

(ii) Non-flammability: unlike many organic solvents, ILs are highly resistant to combustion.

(iii) Extreme stability: ILs are remarkably stable over a wide range of pH and temperature conditions, making them suitable for harsh environments.[74]

(iv) Long-term stability: ILs do not decompose readily, which enhances long-term sustainability.

(v) Amphiphile self-assembly: ILs can be used to create self-assembled structures with unique properties that can be exploited in various applications, such as drug delivery and nanotechnology.

(vi) High dissolving power: ILs are excellent solvents for various organic and inorganic compounds, including gases, such as H_2, CO, and CO_2.[75]

These impressive properties have opened up a vast range of potential applications for ILs in various sectors, as follows.

(i) Green solvents: ILs are explored as replacements for traditional solvents in various chemical processes, offering a more sustainable and environmentally friendly alternative.[76]

(ii) Energy storage: ILs are investigated for use in batteries, fuel cells, and other energy storage devices due to their high ionic conductivity and stability.[77]

(iii) Pharmaceuticals: ILs are used to develop new drugs and drug delivery systems, taking advantage of their unique properties.[38]

(iv) Catalysis: ILs can be used as catalysts in various chemical reactions, offering improved efficiency and selectivity.[78]

(v) Separation technologies: ILs are used to develop new and improved methods for separating and purifying various chemicals and materials.[79]

(vi) Lubricants: ILs are investigated as lubricants for high-temperature and high-pressure applications due to their exceptional thermal stability and low volatility.[80]

The various applications of ILs are pictorially depicted in Fig. 4. Research on ILs is growing rapidly, and new applications are being discovered all the time. With their unique properties and vast potential, ILs are poised to revolutionize various industries and contribute significantly to a more sustainable future. Because only about 300 ILs are currently commercialized, one can imagine how many opportunities in this field remain untapped and why this field of chemistry is so alluring.[72] Despite the notable advancements, the cost still stands as an obstacle and restricts most applications to specialized, small-scale implementations.[81]

5. ILs as a revolutionary choice over organic corrosion inhibitors

ILs offer several advantages over other organic corrosion inhibitors, making them a preferred choice for various applications. Here are some key explanations for preferring ILs:

(i) High thermal stability: ILs exhibit superior thermal stability, often withstanding temperatures exceeding 200 °C. This makes them suitable for high-temperature corrosion inhibition applications where conventional inhibitors may degrade or decompose.[82]

(ii) Low vapour pressure: ILs generally have very low vapour pressures, minimizing evaporation and inhalation hazards. This is particularly important in confined spaces or when working with volatile organic compounds (VOCs).[83]

(iii) Tunable properties: by selecting appropriate combinations of cations and anions, the characteristics of ILs can be tuned. This allows for fine-tuning of properties, such as viscosity, miscibility, and solubility, enabling better surface protection applications.[84,85]

(iv) High solubilities: ILs often exhibit high solubilities in a wide range of solvents, including water, organic solvents, and supercritical fluids. This versatility makes them applicable as corrosion inhibitors in various environments and on different substrates.

(v) Adsorption and film-forming propensity: ILs have a strong affinity for metal surfaces, allowing them to form a protective barrier that hinders corrosion reactions. This adsorption ability is enhanced by the presence of specific cations and anions.[86] ILs can form thin, stable films on metal surfaces, providing long-lasting protection against corrosion.[86,87]

(vi) Synergistic effect: ILs can be combined with other corrosion inhibitors to induce synergistic effects, resulting in enhanced protective ability.

(vii) Reusability: ILs can often be recovered and reused, making them a more cost-effective solution than disposable organic inhibitors.

(viii) Versatility: ILs can be used as corrosion inhibitors for a wide range of metals, including carbon steel, stainless steel, copper, aluminium, and magnesium. An extensive variety of metals, including carbon steel, stainless steel, copper, aluminium, and magnesium, can be protected from corrosion damage by the application of ILs.

(ix) Eco-friendliness: many ILs are considered more environmentally friendly than traditional organic inhibitors due to their lower toxicity and biodegradability.[88]

6. A comprehensive analysis of the anti-corrosive performance of N^+-based ILs for steel substrates

The advent of ILs has introduced a new era of corrosion inhibition, offering a radiant shield against the relentless

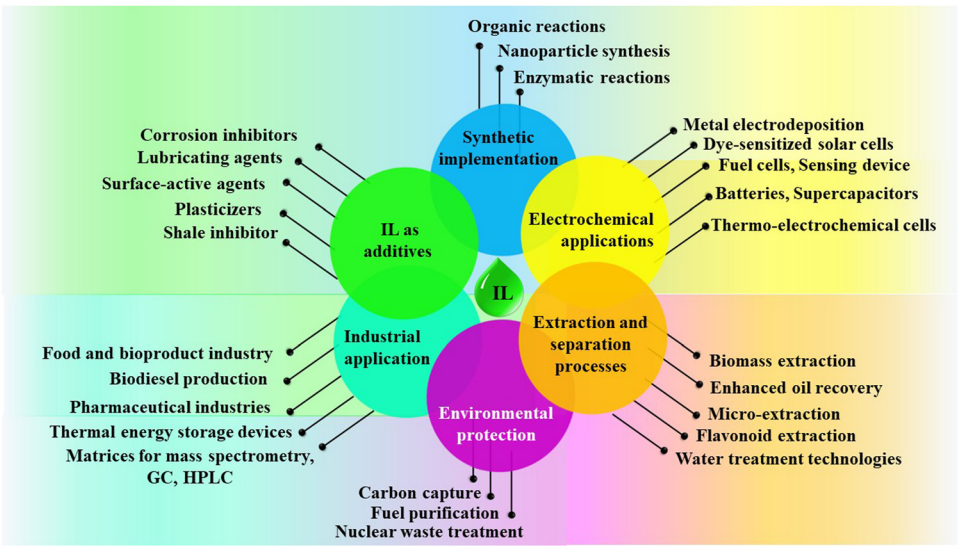

Fig. 4 Pictorial representation of the diverse applications of ILs.

degradation of iron metals and alloys. Pioneering experimental techniques have illuminated the intricate mechanisms underlying the anti-corrosive prowess of ILs, paving the way for a transformative era in safeguarding metallic structures.

As demonstrated in Fig. 5, several imperative factors significantly affect the adsorption process of ILs onto metal surfaces: the nature of the constituent ions, the presence of specific functional groups, such as –COOH, $–SO_3H$, $–NH_2$, and –OH, and the number and length of alkyl chains.

Aromatic moieties and the presence of external ions can further enhance this process, resulting in synergistic effects.

The cationic part of the IL plays a key role in anchoring the IL film to the metal surface, forming strong bonds through chemisorption. However, non-bonding electrons of heteroatoms and the π-electron cloud of aromatic moieties facilitate physisorption, further strengthening the adhesion of the film on the metal. Existing alkyl groups within the molecule with their hydrophobic nature act as a barrier against the corrosive ingredients present in the exposed environments. As the length and number of carbon chains increase, the hydrophobicity of the film becomes more pronounced, providing a robust barrier property.

Understanding the intricate interplay of these factors is crucial for designing and developing ILs with optimal corrosion inhibition properties. Recent advancements in research have shed light on the exciting potential of N^+-containing ILs in this regard. These ILs, with their unique structural features, offer enhanced adsorption capabilities and superior film-forming properties, making them even more effective corrosion inhibitors for iron alloys, specifically steel surfaces.

In this discussion, five types of N^+-based ILs (*e.g.*, ammonium, pyridinium, piperidinium, pyrrolidinium, and imidazolium cation containing ILs) have emerged as potential contenders in the field of steel protection from corrosion in various aggressive mediums. This comprehensive exploration is illuminated by advanced analytical techniques that provide a comprehensive understanding of their efficacy in corrosion inhibition.

(i) Ammonium-based ILs (AmILs): these types of ILs are characterized by the presence of an ammonium-based cation and an appropriate anion. The cationic part of AmILs usually consists of 1°,2°,3° or 4° ammonium cation, and the anionic parts can be varied as Cl^-, sulfonate ($–SO_3H$), and $HCOO^-$. AmILs are known for their excellent film-forming ability, which acts as a physical barrier, hindering access to corrosive agents penetrating the metal surface.

(ii) Piperidinium-based ILs (PiILs): these ILs combine the advantages of both pyridinium and ammonium-based ILs. The piperidine ring structure offers a stronger adsorption ability than ammonium while maintaining the film-forming capacity.

(iii) Pyridinium-based ILs (PyILs): the heterocyclic structure of the pyridinium cation provides a strong adsorption ability because of the presence of a lone pair of electrons on the N-atom. This leads to a strong chemisorption of PiILs with the metal surface, enhancing the efficacy of the ILs as a corrosion inhibitors.

(iv) Pyrolidinium-based ILs (PyrILs): similar to piperidinium ILs, these ILs also possess a five-membered nitrogen-containing ring. However, the presence of an additional carbon atom in the ring leads to increased hydrophobicity, further enhancing the effectiveness of the protective film.

(v) Imidazolium-based ILs (ImILs): these are the most extensively studied N^+-based ILs for corrosion inhibition. The presence of two nitrogen atoms in the imidazole ring allows for multiple adsorption sites, leading to a robust and long-lasting interaction with the metal surface. Additionally, the aromatic character of the imidazolium cation contributes to its excellent thermal stability, making it suitable for high-temperature applications.

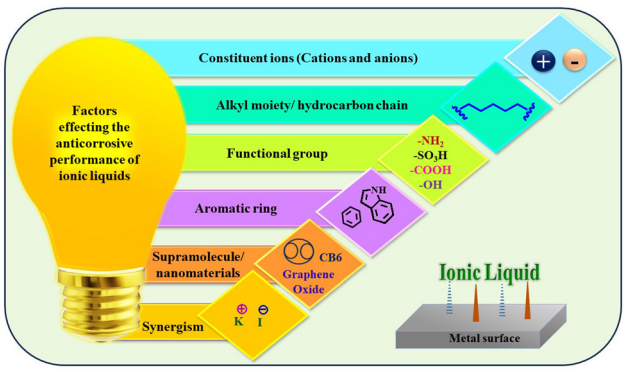

Fig. 5 Key factors that regulate the corrosion inhibition performance of ILs.

6.1. AmILs as anticorrosive agents

AmILs have emerged as promising green alternatives in the field of corrosion mitigation strategies. These ILs, composed of ammonium cations paired with various anions, exhibit unique properties that make them effective anticorrosive agents. The remarkable ability of AmILs to form a stable barrier film on metal exteriors significantly impedes corrosion processes.[89–91] The ionic nature of these compounds facilitates their interaction with metal surfaces, forming a robust barrier that hinders the penetration of corrosive agents. Additionally, the tunable nature of AmILs allows for the customization of their chemical structure to enhance specific anticorrosive properties, making them adaptable to diverse industrial applications.[92] Their low volatility, thermal stability, and negligible vapour pressure contribute to their suitability for corrosion protection in various environments. As researchers continue to explore and optimize the use of AmILs, their application as anticorrosive agents holds great promise for advancing corrosion control strategies while aligning with the increasing demand for sustainable and eco-friendly solutions.[93,94]

In several sub-classes of ILs, the AmILs have demonstrated exceptional anti-corrosive activity. The chemical constituents of cations are mostly responsible for their anticorrosive effectiveness. Several studies have revealed that the inhibitory mechanism of AmILs is predominately based on the physisorption process of ILs onto metallic substrates. Additionally, AmILs

have several advantages over other ILs, including surfactant nature, reduced toxicity compared to heterocyclic group-based ILs, cost-effectiveness, and less tedious synthesis procedures, that provide high-purity reaction products. Another important feature of AmILs is their 'tensioactive property', *i.e.*, the property by which a chemical species containing polar and non-polar moieties can change the value of surface tension.[90]

Effect of ions. The constituent ions of the IL stunning play a role in retarding the rate of metallic corrosion. Generally, the constituent ions of the ILs are adsorbed onto the metal plane *via* electrostatic interaction and form an effective barrier film on the surface of exposed metals. The effectiveness of benzalkonium chloride (BKC) AmILs for protecting carbon steel against 0.1 M H_2SO_4 medium was recently described by Guo *et al.*[95] Fig. 6(a) illustrates the change in impedance value of carbon steel in H_2SO_4 medium without and with the gradual addition of BKC. All the acquired impedance spectra clearly display a single and slightly depressed semi-circle loop, suggesting that the electrochemical nature of the metal–electrolyte interface does not exhibit ideal capacitive behaviour. The deviation from pure semi-circle behaviour is attributed to surface roughness and surface inhomogeneity that occurred during corrosion. Herein, the equivalent circuit used to fit the Nyquist plots is presented in Fig. 6(b). The rate of corrosion is determined by the charge transfer resistance (R_{ct}) that corresponds to the resistance between the metal and outer Helmholtz plane (OHP). Cl^- ions play a significant role in the formation of the IL film. The Cl^- ions have a higher propensity to get adsorbed on metal surfaces than SO_4^{2-} ions due to their lower degree of hydration. This feature leads to the accumulation of extra negative charges along the interface and ultimately facilitates greater adsorption of the cations. The Cl^- ions act as a bridge in the metal–BKC interface to facilitate adsorption to a greater extent. However, a coordinate bond could arise as a result of partial electron transference from the benzene ring of BKC to the unoccupied d-orbits of iron. Accordingly, BKC cations occupy the available positions on the free metal surface and are adsorbed strongly on the metal surface, thereby hindering the attack of aggressive SO_4^{2-} ions. Additionally, a recent patent (AU2021204283B2) disclosed the anticorrosive performance of a series of AmILs with one hydrophobic group and two identical hydrophilic groups.[96] AmILs acted as efficient corrosion inhibitors for protecting 1018 carbon steel in the presence of a brine solution. It was observed that the di-cationic or di-anionic AmILs are more efficient than the traditional AmILs.

Effect of aromatic moieties. The type of aromatic moieties within IL significantly affects the corrosion suppression nature of the ILs. The π-bonded electrons of the aromatic moiety are involved in electron donation from ILs to vacant metal orbitals, which in turn facilitates the chemisorption process of ILs onto the substrate. According to a recent study, three choline amino acid AmILs, namely choline tyrosine ([Ch][Tyr]), choline phenylalanine ([Ch][Phe]), and choline tryptophan ([Ch][Trp]), were chosen as the desired material for the retardation of mild steel corrosion in the presence of a 1 M HCl solution.[97] According to the results of the potentiodynamic polarization studies, AmILs performed as mixed corrosion inhibitors because they had an impact on both the cathodic and anodic reaction processes. The dynamic potential polarization curves of mild steel electrodes immersed in 1 M HCI without and with varying concentrations of AmILs at 298 K did not significantly change in nature. However, the corrosion current density (i_{corr}) does significantly decrease with the addition of higher concentrations of AmILs. This phenomenon clearly sheds light on the fact that the anodic reaction (*i.e.*, metallic dissolution) and cathodic reaction (*i.e.*, hydrogen evolution reaction) processes are reduced by the application of corrosion inhibitors. Simultaneously, the corrosion reaction rate is reduced without changing the metal corrosion reaction mechanism. The slopes of the Bode impedance graphs indicate that the middle frequency has a negative value with an absolute value of less than 1, whereas the lower and higher frequency sections have flat responses. This suggests that the circuit has a non-ideal capacitor part that contributes to a negative slope. Scanning electron microscopy

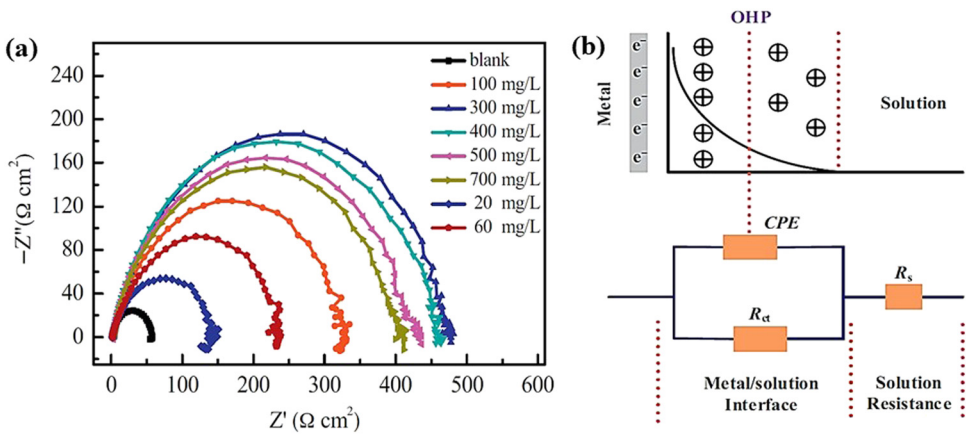

Fig. 6 (a) Nyquist plot for the carbon steel working electrode in the presence of 0.1 M H_2SO_4 solution without and with different concentrations of BKC, (b) potential distribution diagram at the interface between the metal and the electrolytic solution (above) and analogous circuit used to fit the Nyquist plot (bellow) [reprinted with permission from ref. 95, ©2015 Elsevier].

(SEM) and energy dispersive X-ray spectroscopy (EDS) studies were performed to understand the structural variations before and after the use of AmILs. It is clear that the anions are mainly responsible in this case for the excellent adsorption capability of the ILs onto the metallic surface. AmILs cover the outer surface of the metal by forming a monolayer adsorption film that prevents the metal from interacting with an adverse environment. There is a diminishing tendency of electrochemical reactions (cathodic and anodic), resulting in a reduction in electron transfer on metal surfaces. Moreover, the adsorption of the AmILs leads to the displacement of Cl^- ions pre-adsorbed onto mild steel, *i.e.*, the desorption of Cl^- occurs. [Ch][Phe] exhibited maximum corrosion inhibition efficacy because of the presence of a phenyl moiety. The reduced corrosion inhibition efficacy of [Ch][Trp] may be triggered by the additional hydroxyl on the benzene rings, which reduces their aromatic symmetry rather than increasing the molecular active site. In the case of [Ch][Tyr], the enhanced aromatic nature of the indole moiety reduces the electron-donating nature of [Ch][Tyr]. Consequently, its corrosion inhibition efficiency (IE) is reduced to a greater extent, resulting in the following order of effectiveness for metal protection: [Ch][Phe] > [Ch][Trp] > [Ch][Tyr].

Effect of alkyl chains. Alkyl chains are generally hydrocarbon groups. From the literature survey, it is found that the alkyl chains are responsible for introducing hydrophobic characteristics within the corrosion inhibitor. Moreover, an increment in alkyl chain length can cover the underlying surface to a greater extent. It is noteworthy that after a certain range, enhancement in alkyl chain length may reduce the surface coverage area due to the agglomeration of ILs. Subsequently, the protective performance of ILs is greatly influenced by the presence of alkyl chains. In this context, *N*-trioctyl-*N*-methyl ammonium (TMA) methylsulfate and *N*-tetradecyl-*N*-trimethyl ammonium (TTA) methylsulfate are two intriguing AmILs that were investigated by Lozada and co-workers to understand the ability of the studied ILs to mitigate corrosion of carbon steel (API-X52) in HCl solution.[90] Considering the organic origin, simple synthetic pathway and minimal toxicity, the methylsulfate ion was preferred as the anionic counterpart. The metal surface was kept in direct contact with a 1 M HCl solution with various dosages of AmILs, temperatures, and immersion periods to assess the effectiveness of the AmILs using electrochemical analytical techniques. It was observed that the corrosion inhibitors had an impressive anticorrosive activity at 40 °C. The IE obtained from PDP (IE_{PDP} %) *vs.* concentration graphs for TMA and TTA at various immersion periods and temperatures, as displayed in Fig. 7, demonstrate how the IE_{PDP} increases with the increase in concentration. The systems depicted in Fig. 7(a) during 0.3 hours of immersion exhibited comparatively higher IE_{PDP} values than those immersed during 12 hours. This phenomenon can be attributed to the partial desorption process of ILs promoted by the immersion duration. Nevertheless, in comparison to the studied temperatures, the maximum IE_{PDP} values were observed at 40 °C after 12 hours of immersion. However, as shown in Fig. 7(b), the TTA inhibitor exhibited a similar effect. Inhibition efficiency values are often lower than

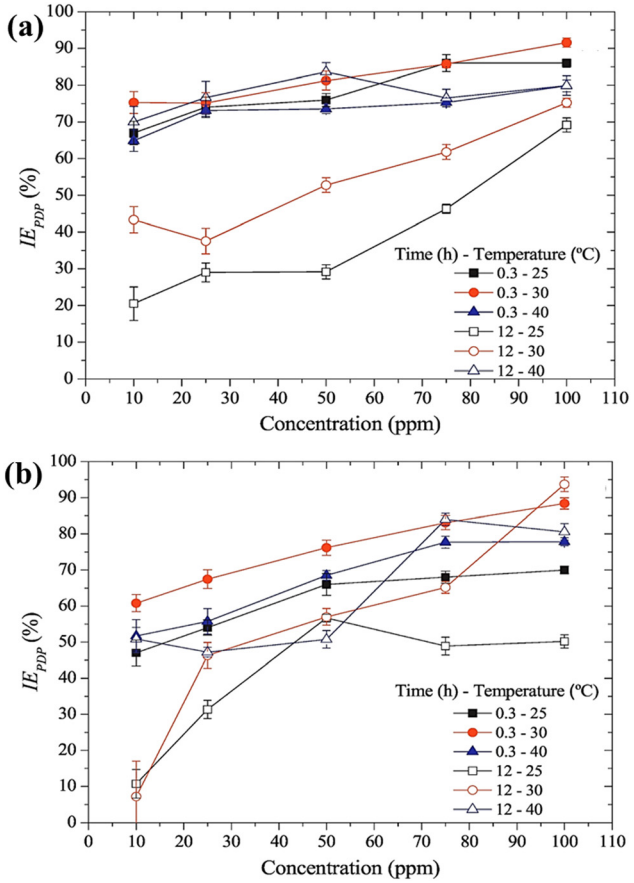

Fig. 7 After evaluating API-X52 steel as a working electrode in the presence of 1 M HCl solution, the inhibition efficiency of (a) TMA and (b) TTA as functions of the immersion duration and temperature [reprinted with permission from ref. 90, ©2018 Elsevier].

those of TMA ILs, whereas this type of action is more pronounced at low concentrations and longer immersion durations. Additionally, X-ray photoelectron spectroscopy (XPS) analysis demonstrated the adsorption of AmILs (*e.g.*, TMA and TTA) on the metal surface. Within the cationic moieties of TMA and TTA, there are one and three methyl groups, respectively. Generally, short-chain alkyl groups are supposed to increase the volume of the polar groups. By increasing the number of short-chain alkyl groups, the adsorption effectiveness of TTA causes steric crowding to develop at the polar head position to decrease considerably because of the predominant steric hindrance created on the hydrophilic part of the TTA scaffold. This feature leads to a reduction in the adsorption effectiveness of TTA compared to that of TMA.

Another two AmILs, namely glycine propyl ester lauryl sulphate ($GlyC_3LS$) and glutamic acid propyl ester lauryl sulphate ($GluC_3LS$), were synthesized, and their protective capability was thoroughly investigated by Zehra *et al.*[98] In this study, mild steel was used as the target metal, and 1 M HCl was used as the electrolytic solution for the corrosion inhibition studies. The adherence of both the studied AmILs on the metal surface occurs through both physisorption and chemisorption processes; subsequently, the IE reaches 99.81% (in electrochemical

impedance spectroscopy *i.e.*, EIS or potentiodynamic polarization *i.e.*, PDP). Because of the variation in the cationic parts of the two ILs, $GluC_3LS$ acted as a better inhibitor than $GlyC_3LS$, as supported by electrochemical and theoretical analyses. The additional hydrocarbon chain attached to the –COOH functional group within $GluC_3LS$ facilitates strong adsorption on the test sample.

Effect of supramolecular architecture. Berdimurodov *et al.* were the first to introduce a new type of cucurbit [6]uril-based [3]rotaxane supramolecular IL (denoted as CB6-based[3] rotaxane) as a green corrosion inhibitor.[97] The supramolecular structure of CB6 contains a giant planar structure with many electron-rich heteroatoms. These electron-rich sites further participate in electron donation. This IL exhibited effective corrosion inhibition performance to protect carbon steel within a mixture of NaOH and NaCl in the same molar ratio (1 : 1). The presence of the supramolecular part enhanced the water solubility of the IL. In that reported work, EIS, PDP, cyclic voltammetry (CV), and electrochemical noise measurement (EN) were executed for electrochemical investigations of corrosion inhibition studies. Consequently, it was revealed that the anticorrosive efficiency reached up to 97.97% with the application of a 100 mg L^{-1}/0.032 mM concentration of IL. From the CV experiment, it was found that the oxidation curve diminished with the addition of CB6-based [3]rotaxane within 1 M NaOH and 1 M NaCl solution. The reduction reaction on the metal electrode occurs before 0.3 V in the alkali medium without an inhibitor. The outcomes indicate retardation in the reduction reaction, which is a diminished rate in the hydrogen evolution reaction. To evaluate the change in electrochemical noise, an EN experiment was performed for the carbon steel sample without and with various concentrations (25, 50, 75 and 100 mg L^{-1}) of CB6-based [3]rotaxane in a 1 M NaOH + 1 M NaCl solution mixture for a duration of 900 minutes, as shown in Fig. 8.

The experimental results clearly indicate that the potential and current noise for inhibitor-free steel samples were significantly in the higher (more positive) potential and current regions. This fact can be attributed to the presence of free OH^- and Cl^- ions because of their less noise resistance. This outcome indicates a higher rate of corrosion. However, the electrochemical noise is reduced to the lower (more negative) region of potential and current in the presence of IL. This phenomenon leads to a decrease in the corrosion current and potential value with the addition of IL. $\bar{R}_{rms}$ values, which denote the degree of inhibition efficacy, were calculated from the EN experiments. The low value of $\bar{R}_{rms}$ (136.3 Ω) for the IL-free system indicates less inhibition, which means more corrosion. This phenomenon also leads to a decrease in the corrosion current and potential value with the addition of IL. The $\bar{R}_{rms}$ value increased significantly with the addition of the IL in the aggressive electrolyte solution, indicating better corrosion resistivity. The 100 mg L^{-1} of the supramolecular IL in the electrolyte mixture showed 97.33% IE, as obtained from EN experiments. The amount of charge transfer from the anodic region to the cathodic region on the working electrode surface was significantly low in the presence of IL.

The role of this supramolecular IL in protecting low carbon steel in the presence of NaOH and NaCl mixture is illustrated in Fig. 9. The corrosion process of metals studied by 1 M NaOH and NaCl electrolytic solutions is a complex phenomenon. The OH^- and Cl^- ions are adsorbed primarily on the Fe surface.

When IL is added to the solution, the adsorbed OH^- and Cl^- ions are neutralized by the protonated N atoms of the IL. This phenomenon is considered a physisorption process *via* physical interaction or electrostatic interaction. However, the p-orbital electrons of N and π orbital electrons are transferred to the vacant d-orbital of Fe. These is termed chemisorption. Again, d-orbital electrons from Fe are transferred to the vacant π-orbital of CB6-based [3] rotaxane, *i.e.*, retro-donation occurs.

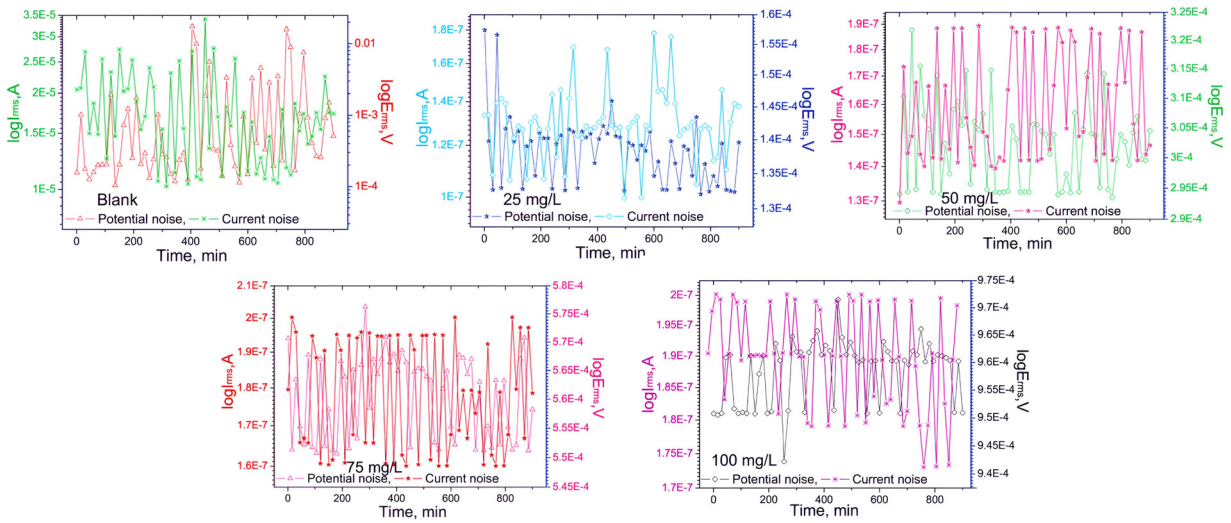

Fig. 8 Electrochemical noise measurement of carbon steel in a solution of 1 M NaOH + 1 M NaCl, both with and without the CB6-based [3]rotaxane inhibitor. [Reprinted with permission from ref. 97, ©2022 Elsevier.]

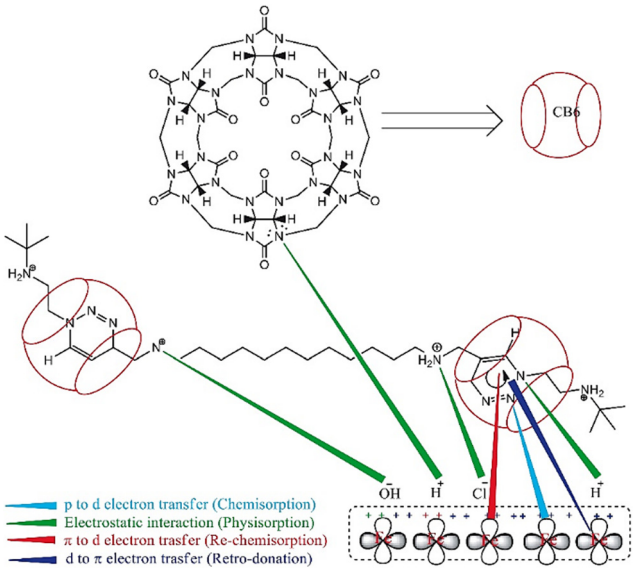

Fig. 9 Schematic illustration of the protective mechanism of CB6-based [3]rotaxane to retard the rate of corrosion of low-carbon steel in 1 M NaOH + 1 M NaCl [reprinted with permission from ref. 97, ©2022 Elsevier].

The corrosion inhibition performances of some AmIL-based inhibitors are tabulated in Table 1.

6.2. PiIL as an anticorrosive agent

PiILs are the category of ILs in which a nitrogen-containing six-membered heterocyclic ring is present along with a positive charge centred on nitrogen. PiILs are emerging as a groundbreaking class of corrosion inhibitors, exhibiting exceptional efficacy and environmental compatibility. These innovative molecules, characterized by their piperidinium cations paired with various anions, offer a unique approach to combat corrosion, which is a ubiquitous and costly problem across diverse industries. Their potent anticorrosive action stems from their remarkable film-forming capability.[45] PiILs are readily adsorbed onto the metal surface, leading to a robust, adherent layer that serves as an impenetrable barrier for corrosive agents, such as oxygen, chloride ions, and acidic solutions.[100] This effectively shields the underlying metal from corrosive attack, drastically decreasing the corrosion process and extending the operational lifespan of valuable assets. Unlike traditional corrosion inhibitors, which often rely on volatile and potentially hazardous components, PiILs are engineered for sustainability. Their low volatility and negligible vapour pressure significantly reduce their environmental impact, minimizing the risk of air and water contamination. Furthermore, their inherent biodegradability provides an added advantage of environmental responsibility, aligning with the increasing demand for eco-friendly solutions. Beyond their environmental benefits, PiILs offer exceptional versatility and tunability. The chemical structure of these ILs can be readily tailored by modifying the cation or anion, enabling researchers to fine-tune specific properties, such as adsorption strength, thermal stability, and solubility. This customizable nature of PiILs allows for the development of tailor-made corrosion inhibitors for diverse applications, ranging from protecting pipelines and storage tanks in the oil and gas industry to safeguarding aircraft components and medical implants. The impressive performance and environmental advantages of PiILs have ignited widespread interest in corrosion research. Their emergence marks a significant step towards a sustainable future where valuable assets are safeguarded effectively and responsibly, ushering in a new era of corrosion control strategies.[101] PiILs play a crucial role in the field of IL-based corrosion mitigation strategies.

Combined effects of chain length and synergism. In corrosion chemistry, the term 'synergism' defines the enhancement in corrosion inhibition efficacy by the addition of another species. When two or more species exhibit different corrosion mitigation rates but their combined effect shows better IE than the sum of their corrosion inhibition, this effect is called a synergistic effect. In the context of synergism, Singh *et al.* reported the anticorrosive behaviour of three commercially available PiILs, namely, 1-methyl-1-propylpiperidinium bromide (IL-1), 1-butyl-1-methylpiperidinium bromide (IL-2), and 1-butyl-1-methylpiperidiniumbis(trifluoromethanesulphonyl)imide (IL-3), for protecting Q235 grade steel in the presence of 1 N HCl.[100] Interestingly, the incorporation of potassium iodide (KI) salt significantly increases the protective nature of the PiILs. Electrochemical analysis techniques, such as EIS and PDP, indicated better corrosion inhibition effectiveness for IL-3 (97.4%), followed by IL-2 (94.7%) and then IL-1 (91.3%) for 400 mg L^{-1} concentration. This result infers that the effectiveness of corrosion inhibition in IL-2 is higher than that of IL-1 due to the presence of an additional hydrocarbon group. Moreover, in the case of IL-3, additional carbon, such as IL-2, and an additional larger anionic moiety facilitate better electrostatic interaction with the metal plane. The study revealed that IL-3 exhibited a higher corrosion suppressing nature compared to IL-2, followed by IL-1. This finding could be useful in developing more effective anti-corrosion measures. Nevertheless, a mere addition of 0.5 mM KI resulted in a significant boost in protective performance. IL-1 protection surged to 95.2%, IL-2 to 98.2%, and an impressive 99.1% for IL-3. It can be said that the presence of I^- facilitates electrostatic interaction between the cations of ILs and the underlying positively charged steel surface.

6.3. PyIL as an anticorrosive agent

A positively charged six-membered ring comprising 5 carbon atoms and 1 nitrogen atom renders the structure of the heterocyclic pyridinium cation consisting of six delocalized π-electrons within the conjugated cyclic structure. In the domain of the IL-based corrosion inhibition strategy, PyILs play a pivotal role.[35,102]

Effect of chain length. The effects of chain length can be successfully explained in the following notable studies. The corrosion inhibition effectiveness of 1-ethyl-4-(2-(4-fluorobenzylidene)hydrazinecarbonyl)pyridin-1-ium iodide (IPyr-C_2H_5) and 1-butyl-4-(2-(4-fluorobenzylidene)hydrazinecarbonyl) pyridin-1-ium iodide (IPyr-C_4H_9) was thoroughly investigated for mild steel surfaces in a 1 M HCl electrolyte solution.[103] The anticorrosive effectivity of this PyIL was analyzed using

Table 1 AmIL as anticorrosive additives for the protection of steel surface from corrosion

Sl. no.	Ionic liquid (Structure and IUPAC name)	Metal surface/ medium	Adsorption mechanism	Isotherm model	Highlights	Ref.
1	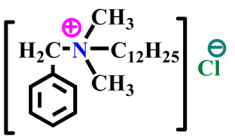 Benzalkonium chloride (BKC)	Carbon steel/ 0.1 M H_2SO_4	Both physisorption and chemisorption	Langmuir	(i) IE reaches 88.34% (EIS) and 83.52% (PDP)@ 300 mg L^{-1} (ii) The presence of Cl^- ions increased the adsorption capability of the AmIL on the carbon-steel surface through bridging (iii) The presence of a long alkyl chain facilitates extra surface coverage	95
2	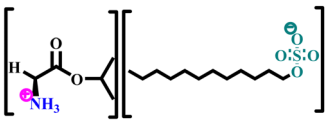 $GlyC_3LS$ 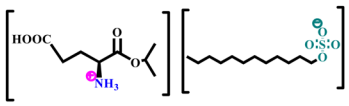 $GluC_3LS$	Mild steel/1 M HCl	Both physisorption and chemisorption	Langmuir	(i) IE of these biodegradable amino acid-based ILs: 98.64% for $GlyC_3LS$ and 99.81% for $GluC_3LS$@100 ppm at 60 °C (ii) Corrosion inhibition analysis was performed in a wide temperature range (30, 40, 50 and 60 °C) (iii) $GluC_3LS$ shows better corrosion inhibition efficiency than $GlyC_3LS$ because of the combined effect of the hydrocarbon chain and –COOH functional group	98
3	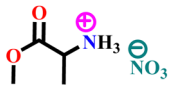 L-alanine methylester nitrate ($LAlaC_1NO_3$)	Mild steel/1 M HCl	Physisorption and chemisorption	Langmuir	(i) Corrosion inhibition analysis was performed in a wide temperature range (30, 40, 50 and 60 °C) (ii) IE: 84% @0.003 M (iii) The presence of heteroatoms facilitates adsorption	42
4	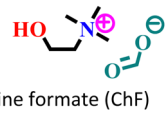 Choline formate (ChF) 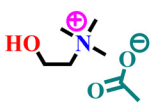 Choline acetate (ChA)	Mild steel/1 M HCl	Mixed adsorption	Langmuir	(i) Corrosion inhibition analysis was performed in a wide temperature range (ii) IE of these ILs: 96.9% for ChF and 99.5% for ChA@2 × 10^{-3} M at 50 °C (iii) The presence of an alyl group facilitates better adsorption in ChA	88
5	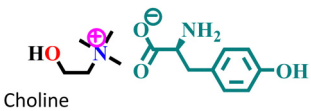 Choline Tyrosine ([Ch][Tyr]) 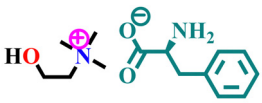 Choline phenylalanine ([Ch][Phe]) 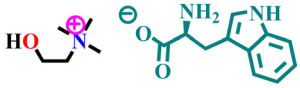 Choline tryptophan ([Ch][Trp])	Mild steel/1 M HCl	Physisorption and predominant chemisorption	Langmuir	(i) IE: [Ch][Phe] > [Ch][Trp] > [Ch][Tyr] (ii) The aromatic nature of the –Ph ring increases the IE, while the decreased aromaticity reduces the IE in the following ILs	99
6	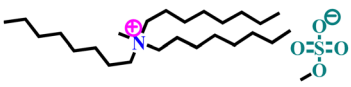 Methyltrioctylammonium methyl sulfate (TMA) 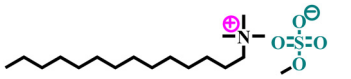 Trimethyltetradecylammonium methyl sulfate (TTA)	API-X52 steel/1 M HCl	Physisorption	Langmuir	(i) IE: TMA > TTA (ii) Increasing numbers of –Me groups facilitate steric crowding in the polar head group in the case of TTA. Accordingly, the adsorption tendency of TTA is diminished compared to that of TMA	90

electrochemical analysis techniques, such as EIS. Different types of adsorption isotherm models, such as Langmuir, Freundlich, Temkin and Frumkin were adopted to interpret the results of the EIS measurements to gain a better understanding of the interaction between PyIL and mild steel in an HCl environment, as illustrated in Fig. 10(a–d).

The Langmuir adsorption isotherm model was the undisputed choice for describing the PyIL adsorption mechanism, which is also supported by the obtained high linear regression coefficients ($R^2 > 0.999$) value. The strong adsorption of the PyILs is depicted by the high value of equilibrium constant (155.57×10^2 M^{-1} for IPyr-C_4H_9 and 218.93×10^2 M^{-1} for IPyr-C_2H_5). These findings suggest that the film formation of PyILs on the metal surface involves both physical and chemical adsorption mechanisms.

The sequential order of inhibitory performance is IPyr-C_2H_5 < IPyr-C_4H_9, which is because of their large specific surface area. The longer carbon chain of IPyr-C_4H_9 facilitates its adsorption on iron surfaces more predominately than IPyr-C_2H_5. On the contrary, Hajjaji *et al.* shed light on the corrosion inhibition effectiveness of two ILs, namely, (*E*)-4-(2-(4-fluorobenzylidene)hydrazinecarbonyl)-1-propylpyridin-1-ium iodide (denoted as Ipyr-C_3H_7) and (*E*)-4-(2-(4-fluorobenzylidene) hydrazinecarbonyl)-1-pentylpyridin-1-ium iodide (denoted as Ipyr-C_5H_{11}).[104] The electrochemical results revealed that the synthesized PyILs act as mixed-type inhibitors with a predominant anodic type in nature. Electrochemical investigations, such as EIS and PDP, were performed to analyse the protective capabilities of the PyILs against mild steel corrosion in HCl electrolytes. From the EIS experiments, the obtained increased polarization resistance indicates that the corrosion inhibitors are adsorbed on the metal surface in the metal–electrolyte interface by dislodging previously adsorbed water molecules. The decreased corrosion current density with the addition of ILs obtained from the PDP study reveals the strong adsorption of ILs to the metal surface, specifically the anodic sites. The negatively charged I^- ions are adsorbed on the positively charged metal surface through Coulombic interaction, resulting in a bridge type of linkage formation. This may also be referred to as the occurrence of physisorption. The presence of the aromatic ring, azomethine linkage, and –NH– moiety within the IL scaffold facilitates the sharing of electron clouds with the vacant orbitals of metal atoms, thus resulting in chemisorption. The value of the standard adsorption-free energy ranges from −20 kJ mol^{-1} to −40 kJ mol^{-1}, which signifies the mixed type (*i.e.*, chemical and physical) of the adsorption nature of the ILs. It makes sense that at elevated temperatures, the long chain of Ipyr-C_5H_{11} ILs cannot sufficiently cover the metal surface. With an increase in carbon chain length, the corrosion inhibition efficacy of the current derivatives reaches a maximum when there are four carbons. Consequently, following the elongation of more than four carbons, the inhibitory efficacy gradually starts to decrease.

Similarly, the corrosion suppressing ability of cetylpyridinium picrate (CPP) IL on a mild steel working electrode in the presence of 1 M HCl is another approach of PyIL aspects.[15]

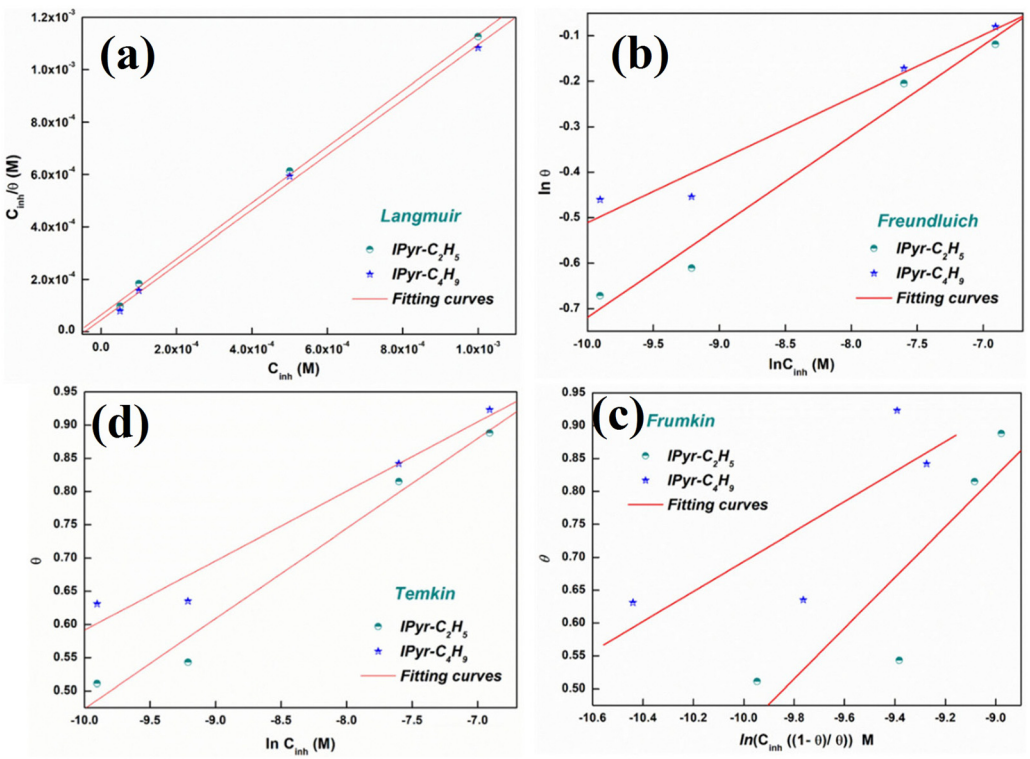

Fig. 10 (a) Langmuir, (b) Freundluich, (c) Frumkin and (d) Temkin isotherm models for understanding the adsorption mechanism of IPyr-C_2H_5 and IPyr-C_4H_9 on mild steel surface in the presence of 1 M HCl at 298 K. [Reprinted with permission from ref. 103, ©2020 Elsevier.]

Gravimetric analysis revealed that the effectiveness of the CPP ILs increased with concentration and test solution temperature, culminating at 99.04% at 70 °C when the concentration was very low or close to 8×10^{-7} M, which was further supported by EIS and PDP analyses. XPS and SEM surface morphology investigations validated the development of a hydrophobic organic–inorganic hybrid protective film. This was the main factor in the strong adsorption of the IL onto the metal surface. The strong binding energy (443.63 kcal mol^{-1}) obtained in the MD simulation study is predominantly attributed to the electrostatic interaction between the IL and the pre-adhered chloride ions onto the metal surface. The D–A interaction between the heteroatoms and aromatic moieties within the ILs and the metal surface helps in the strong adsorption of the ILs, and a self-assembled layer is formed on the metal plane. In addition, the longer cetyl chain within the CPP IL triggered a hydrophobic nature. Consequently, the electrolyte and metal surface were restricted from making contact. The hydrophobic nature induced by the cetyl chain was ascertained from a contact angle (CA) study. At 30 °C, the CA values of polished mild steel and mild steel after immersion in an acidic solution were found to be 53° and 46°, respectively. The addition of CPP IL into the corrosive solution increased the CA up to 92°, which reflects the hydrophobic nature of the steel surface.

Effect of aromatic moiety. A recent study has revealed the fascinating effect of aromatic rings on the protective nature of ILs against metallic corrosion in a neutral medium. Herein, the effect of the aromatic ring on the corrosion retardation of two PyILs, namely, dodecyl pyridinium chloride (DDPC) and dodecyl quinolinium chloride (DDQC), for the protection of X65 carbon steel was explained nicely.[105] Apart from SEM, EDS and atomic force microscopy (AFM), a scanning Kelvin probe (SKP) study was utilized for morphological analysis and roughness measurement of the surface under investigation. Following the gravimetric analysis, the metal samples were removed from the electrolytic medium, and the metal surface was soaked using filter paper.

The surface was then desiccated in a nitrogen environment. The SKP system (SKP5050, KP Technology) was used to obtain surface Volta potential maps of the metal samples through SKP measurement. The SKP is a precise and non-destructive method that provides surface information about electrodes. This technique is renowned as a non-contact process and can analyze potential distribution, measure electrochemical properties, and detect localized corrosion topographies of metals. SKP analysis is conducted in various environments, such as vacuum, open-air, and even humid environments. During the experimentation, a metallic probe, connected to the instrument, scans across the surface of the metallic sample and calculates the Volta potential (*i.e.*, contact potential difference between the vibrating tip and the metal specimen) by evaluating the alternating current. Fig. 11(a–d) depicts the potential distribution diagrams of the studied samples obtained by SKP before and after the weight loss analysis.

The potential distribution of the specimen prior to immersion was discovered to be less than 1, indicating its original state. In the case of the blank sample, the potential distribution shifted towards a positive value, indicating severe corrosion of its surface. When corrosion inhibitors *viz.*, DDPC and DDQC, were present, it shifted towards negative values. This phenomenon suggests the adsorption of the PyILs onto the metal exterior, thereby suppressing the corrosion process and effective protection of the metal surface.

Furthermore, when comparing the potential distribution diagram of the inhibitors, it was observed that DDQC had a lesser value than DDPC, indicating that DDQC had a more significant effect. This observation is consistent with the results obtained from previous electrochemical studies, such as PDP and EIS, and gravimetric analysis, such as weight loss experiments. Fig. 11(a′–d′) illustrates the relative frequency histogram of the SKP potential distribution for each sample, and the position of these distributions was determined by fitting a Gaussian function. From the fitting analysis, the potential distribution of the polished sample with electrolyte, DDPC, and DDQC was found to be −376 mV, 380 mV, −269 mV, and −304 mV, respectively. The corrosion inhibition performances of some PyIL-based inhibitors are summarized in Table 2.

6.4. PyrIL as an anticorrosive agent

The PyrILs are composed of pyrrolidinium cations and various anions. The PyrILs demonstrate excellent adhesion to metal exteriors and form a durable protective film that inhibits corrosion processes.[108,109] The unique molecular structure of PyrILs contributes to their high thermal stability, low volatility, and strong affinity for metal substrates. This combination of attributes enables them to impede the penetration of corrosive agents effectively, thereby safeguarding metal surfaces from degradation.[110–112] Because PyrILs come from non-renewable resources, it has been shown that their biodegradability and biocompatibility are inadequate.[33] In this context, PyrILs are considered preferable contenders in the domain of corrosion mitigation. L-Proline nitrate IL (denoted as [Pro][NO_3]) was synthesized, and its effectiveness as a green corrosion PyrIL was thoroughly investigated.[33]

Effects of nanomaterials. To explore the effect of nanomaterials on the protection of PyrIL, it has been reported that the presence of nanoparticles, such as graphene oxide (GO) and its modified compounds, might be efficient corrosion-resistant materials. The unique characteristics, including hydrophobicity, large surface coverage, resistance to chemicals, thermal and electrical conductivity, and exceptional mechanical strength, are added advantages for versatile corrosion inhibitors. Accordingly, GO-[Pro][NO_3] nanohybrid was formulated and characterized.[34] It was reported that as the inhibitor concentration was increased, inhibition effectiveness reached 86.5% with a 250 ppm corrosion inhibitor at 333 K. This reported GO-IL nanohybrid exhibited better corrosion resistance properties than the other GO-IL composites at higher temperatures.

6.5. ImIL as an anticorrosive agent

The ImILs represent a significant breakthrough in the field of corrosion protection. The term ImILs refers to the ILs, where

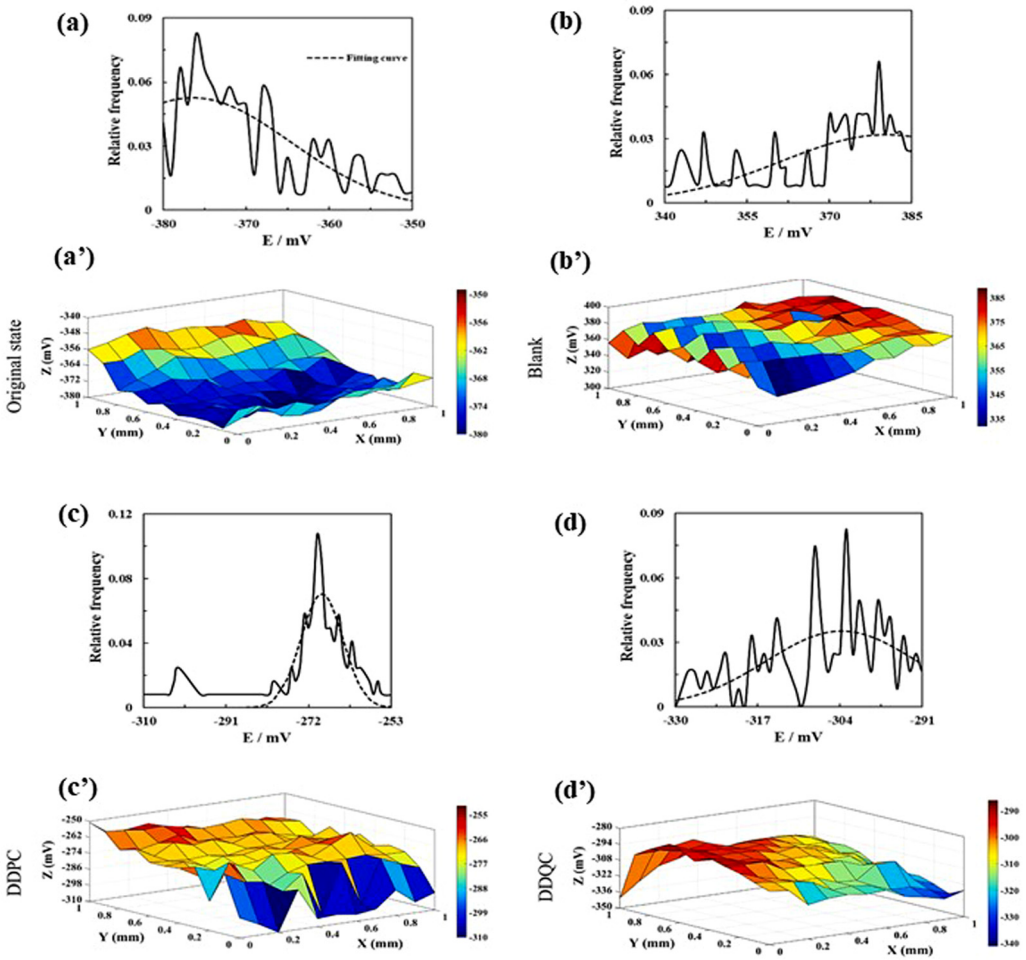

Fig. 11 Relative frequency histogram of SKP diagrams. SKP potential distribution diagrams for carbon steel (a) and (a′) in the original state, (b) and (b′) after being immersed in a sour brine solution, (c) and (c′) with DDPC, and (d) and (d′) with DDQC. [Reprinted with permission from ref. 105, ©2023 Elsevier.]

the imidazole ring contains a positive charge. The imidazole ring was integrated into IL for the first time in 1984, and since then, it has become one of the centrepieces of interest because of its outstanding propensity to yield cationic molten salts (*i.e.*, ILs).[113] These novel compounds, constructed with an imidazolium cation and diverse anions, exhibit exceptional film-forming abilities. This enables them to create a robust and durable barrier on metal surfaces, effectively shielding them from the detrimental effects of corrosion-inducing agents, such as oxygen, chloride ions, and acidic solutions.[88,114–116] Imidazolium salts constitute the most promising subclass of the ILs because their melting point, solubility, conductivity, and viscosity can be tuned by changing the substituents at the nitrogen atoms and counter ions. The imidazole scaffold is a five-membered hetero-aromatic ring containing three carbon atoms and two nonadjacent nitrogen atoms. ILs solely have a high degree of water solubility due to their strong polarity. Recent studies have revealed a considerable augmentation in the application of ImILs as green and protective agents of metal surfaces because of their low toxicity, biodegradability, economic viability and water solubility. The incorporation of the long-chain alkyl group enhances anticorrosive activity by boosting the hydrophobicity of ImILs. It has been conceptualized that the nonpolar alkyl chain (tail part) points towards the bulk electrolyte, while the electron-rich polar hydrophilic imidazolium moiety (head part) adheres to the metallic surface. In the current scenario, ImILs have exquisite applications in the field of corrosion inhibition.[43,117,118] For instance, Guo *et al.* reported an ImIL, namely, 1-dodecyl-3-methyl imidazolium hydrogen sulfate (DMIMHS), as a green corrosion inhibitor for the protection of carbon steel during oil and gas corrosion.[119] CO_2-saturated brine solution (NaCl) was selected as the experimental corrosive medium, and the electrochemical investigations were carried out at 313 K temperature. In the EIS study, it was observed that the capacitive arc diameter increased significantly with the addition of the DMIMHS inhibitor to the electrolytic solution, indicating the protective nature of DMIMHS. The increase in the phase angle peak suggests that frequency dispersion occurs on the electrode surface. It is noteworthy that the curves obtained in the Nyquist plot were not perfectly semicircles, signifying that the metal–electrolyte interface does not possess an ideal capacitive nature. The lack

Table 2 PyILs as anticorrosive additives for the protection of steel surface from corrosion

Sl. no.	Ionic liquid (Structure/IUPAC name)	Metal surface and medium	Adsorption mechanism	Isotherm model	Highlights	Ref.
1	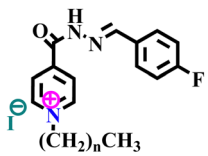 n = 1: 1-ethyl-4-(2-(4-fluorobenzylidene)hydrazinecarbonyl)pyridin-1-ium iodide ($IPyrC_2H_5$) n = 3: 1-butyl-4-(2-(4-fluorobenzylidene)hydrazinecarbonyl)pyridin-1-ium iodide ($IPyr\text{-}C_4H_9$)	Mild steel/ 1 M HCl	Physisorption and chemisorption	Langmuir	(i) IE: 88.8% for $IPyrC_2H_5$ and 92.3% for $IPyr\text{-}C_4H_9$@10^{-3} M and 298 K (ii) The larger chain length of the alkyl group is responsible for the better adsorption of $IPyr\text{-}C_4H_9$	103
2	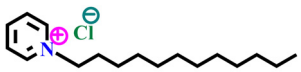 Dodecyl pyridinium chloride (DDPC) 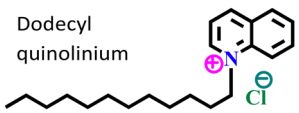 Dodecyl quinolinium chloride (DDQC)	X65 carbon steel/brine solution	Chemisorption	Langmuir	(i) IE: 97.4% for DDPC and 98.3% for DDQC@100 mg L^{-1} and 20 °C in dynamic EIS analysis (ii) The presence of an aromatic ring increased the protective nature of DDQC	105
3	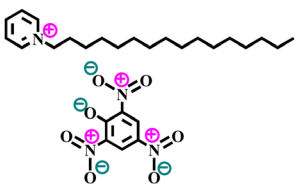 cetylpyridinium picrate (CPP)	Mild steel/ 1 M HCl	Physisorption and chemisorption	Langmuir	(i) IE: 92.34% @8 × 10^{-7} M and 30 °C (ii) Interestingly, the IE increased with an increase in the concentration and temperature because of the formation of the hybrid organic–inorganic protective layer. 99.04% IE was achieved @8 × 10^{-7} M and 70 °C	15
4	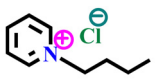 1-Butylpyridinium chloride (BPC) 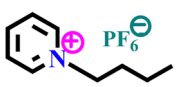 1-Butylpyridinium hexafluorophospate (BPH)	Mild steel/ 15% HCl	Physisorption and chemisorption	Dubinin Radushkevich	(i) IE: 90.3% for BPC and 79.8% for BPH@100 mg L^{-1} and 308 K (ii) The large size of the anion decreases the electrostatic attraction between the IL and the charged metal surface in the case of BPH	35
5	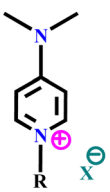 4-(dimethylamino)-1-nonylpyridin-1-ium iodide (4DMN) (when R= C_9H_{19}, X= I) 4-(dimethylamino)-1-(prop-2-yn-1-yl)pyridin-1-iumbromide (4DMP) (when R= CH_2CCH, X= Br)	Carbon steel/3.5 wt% NaCl	Both physisorption and chemisorption	—	(i) IE: 93.8% for 4DMN and 91.9% for 4DMP@5 × 10^{-3} mol L^{-1} and 303 K. (ii) The presence of iodide ions synergistically increased the electrostatic interaction of 4DMN	106

Table 2 (*continued*)

Sl. no.	Ionic liquid (Structure/IUPAC name)	Metal surface and medium	Adsorption mechanism	Isotherm model	Highlights	Ref.
6	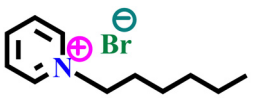 1-hexylpyridinium bromide (NR3)	Carbon steel/1 M HCl	Physisorption as well as chemisorption	Langmuir	(i) IE: 81.3% @3 × 10^{-3} mol L^{-1} and 294 K (ii) Acts as a mixed-type inhibitor	107

of an ideal capacitive nature of the electrode occurs because of the surface roughness, chemical inhomogeneity, and protective layer formation on the electrode. This occurrence is called the frequency dispersion effect. In the Nyquist plot, the radius of the semicircle curve increases, and the time constant value shifts to a smaller frequency zone with the immersion time of the working electrode in the corrosive medium. This outcome reflects the formation of the barrier films of the corrosion product on the working electrode surface. The SEM images of the top surface views may sometimes not provide accurate information regarding the surface of the metal. It was found from the cross-section morphologies of the samples immersed for 48 hours in CO_2-saturated NaCl brine without DMIMHS and for 120 hours with DMIMHS that a layer of corrosion product was formed in the metal-inhibitor interface after the immersion of the targeted metal. With the increase in immersion time, *i.e.*, after immersion of 120 hours, the nature of the corrosion product layer did not change, but the thickness of that film increased significantly.

Effect of functional group. The presence of functional groups has an enormous effect on the adherence properties of ImILs, *vide supra*. In 2020, the protective nature of three ImILs, namely, 1-(2-carboxylic acid) ethyl-3-methylimidazolium hydrogen sulfate, *i.e.*, [(CH_2)COOHMIm][HSO_4], 1-(3-carboxylic acid) propyl-3-methylimidazolium hydrogen sulfate, *i.e.*, [$(CH_2)_2$-COOHMIm][HSO_4], and 1-(4-sulfonic acid) propyl-3-methylimidazolium hydrogen sulfate, *i.e.*, [$(CH_2)_3SO_3$HMIm][HSO_4] for mild steel were investigated in the presence of 0.5 M HCl.[120] In this work, it is nicely investigated how the functional groups, in combination with the alkyl chain length, affect the inhibitory mechanism of ImIL. The IE order of the ImILs are as follows: [$(CH_2)_3SO_3$HMIm][HSO_4] > [$(CH_2)_2$COOHMIm][HSO_4] > [(CH_2)-COOHMIm][HSO_4]. Primarily, the corrosion current density values decreased with the gradual addition of the IL in the range of 1–10 mM, which implies the enhancement of inhibition efficacy. Herein, shortening the hydrocarbon chain of [(CH_2)-COOHMIm][HSO_4] leads to the least corrosion inhibition effectiveness among the three studied ImILs. Interestingly, a further increase in the concentration of the ImILs within the electrolyte solution resulted in a significant decrease in the film formation ability for –COOH-functionalized ImILs and a slight increment for –SO_3H-functionalized ImILs. These phenomena can be attributed to the fact that –COOH-functionalized ImILs have a lower desorption concentration compared to –SO_3H-functionalized ImILs. Additionally, this fact can be attributed to the concentration sensitivity of the –COOH-functionalized ImILs.

Effect of chain length. As previously mentioned *vide supra*, the alkyl chain length of IL significantly affects corrosion inhibition. The effect of chain lengths on ImILs was highlighted by a research team from Egypt.[121] Three ImILs, namely, 3-(2-ethoxymethyl)-1-octyl-1*H*- imidazol-3-ium chloride, 1-decyl-3-(2-ethoxy methyl)-1*H*-imidazol-3-ium chloride and 1-dodecyl-3-(2-ethoxymethyl)-1*H*-imidazol-3-ium chloride designated as IL_1, IL_2 and IL_3 respectively, with different alkyl chain lengths were used as a corrosion suppressive agent for the stainless steel (201 SS) sample in the presence of 2.0 M HCl. Apart from EIS and PDP, another non-destructive electrochemical technique, electrochemical frequency modulation (EFM), was implemented to comprehend the effect of alkyl chain lengths on the corrosive nature of 201 SS. The increased carbon chain length eases the surface coverage of the exposed metal and results in better protection against corrosion. Similar case studies on chain length effects were achieved in the case of 1-vinyl-3-methylimidazolium iodide ([VMIM]I), 1-vinyl-3-proplylimidazolium iodide ([VPIM]I) and 1-vinyl-3- butylimidazolium iodide ([VBIM]I) while protecting steel in acid medium.[122] In another study, Cao *et al.* discussed two task-specific ImILs (namely, 1-(4-sulfonic acid) butyl-3-ethyl imidazolium hydrogensulfate and 1-(4-sulfonic acid) butyl-3-decyl imidazolium hydrogensulfate) designated as C2-IMIC4-S and C10-IMIC4-S with different chain lengths, respectively;[62] they investigated the protective nature of the ImILs towards carbon steel against corrosion. 0.5 M HCl was used as the corrosive medium during the electrochemical experiments. In addition to electrochemical investigations, SEM, XPS, and CA analyses were performed to elucidate the corrosion mitigation effectiveness of the as-synthesized ImILs. The pictorial illustrations of the XPS spectra for Fe 2p, Cl 2p, O 1s, S 2s, N 1s, and C 1s elements on the metal exterior after 24 h of immersion in the absence and presence of 15 mM ImIL in HCl (0.5 M) medium are presented in Fig. 12. As shown in Fig. 12(a), three signals were observed at 709.6 ± 0.1, 710.5 ± 0.1, and 712.1 ± 0.1 eV, which corresponded to Fe $2p_{3/2}$. These peaks were ascribed to Fe^0, ferrous compounds (*e.g.*, FeO and Fe_2O_3), and ferric compounds (*e.g.*, Fe_2O_3, FeOOH and $FeCl_3$), correspondingly. The formation of a robust and insoluble barrier film (Fe_2O_3 and/or FeOOH) impedes the dissolution rate of steel in an acidic environment. The O 1s peaks, as depicted in Fig. 12(b), exhibit two primary peaks. The two

signals are positioned at 529.6 and 531 eV, which are attributable to the O^{2-} and –OH groups of hydrous iron oxides (*e.g.*, FeOOH), respectively. The signal shifts to higher binding energies (530 and 531.4 eV) with the addition of ImILs, indicating a strong interaction between the ImILs. The Cl 2p signals shown in Fig. 12(c) exhibit two signals. One signal at 198.3 ± 0.1 eV signifies the presence of Cl^-, while the other signal at 199.9 ± 0.1 eV denotes $FeCl_3$, indicating the adherence of Cl^- ion onto the metal exterior. Moreover, in the presence of ImILs, the absorption of Cl^- is greater than that in the blank solution. Thus, Cl^- may assist in the adherence of ILs. In the presence of the ILs, two major peaks are observed in the S 2p signal, as shown in Fig. 12(d). The peak at 168.1 ± 0.2 eV corresponds to the Fe–S complex, while the signal at 169.4 ± 0.2 eV is attributed to SO_4^{2-}. The C 1s spectra, as shown in Fig. 12(e), exhibit three signals at 284.7 ± 0.1 (attributable to C–C aliphatic bonds), 285.4 ± 0.1 (associated with C–N), and 288.1 ± 0.1 eV (assigned to C=N). This suggests that the imidazolium counterpart may exist on the steel exterior. The N 1s signals, as depicted in Fig. 12(f), display a signal at around 400.1 eV, which corresponds to the amine group ($–NR_3$).

However, the signal at 401.6 eV is attributed to the quaternary nitrogen (NR_4^+) that indicates a coordinated nitrogen atom and a C–N–Fe bonding. By analyzing the peaks in the C 1s and N 1s spectra

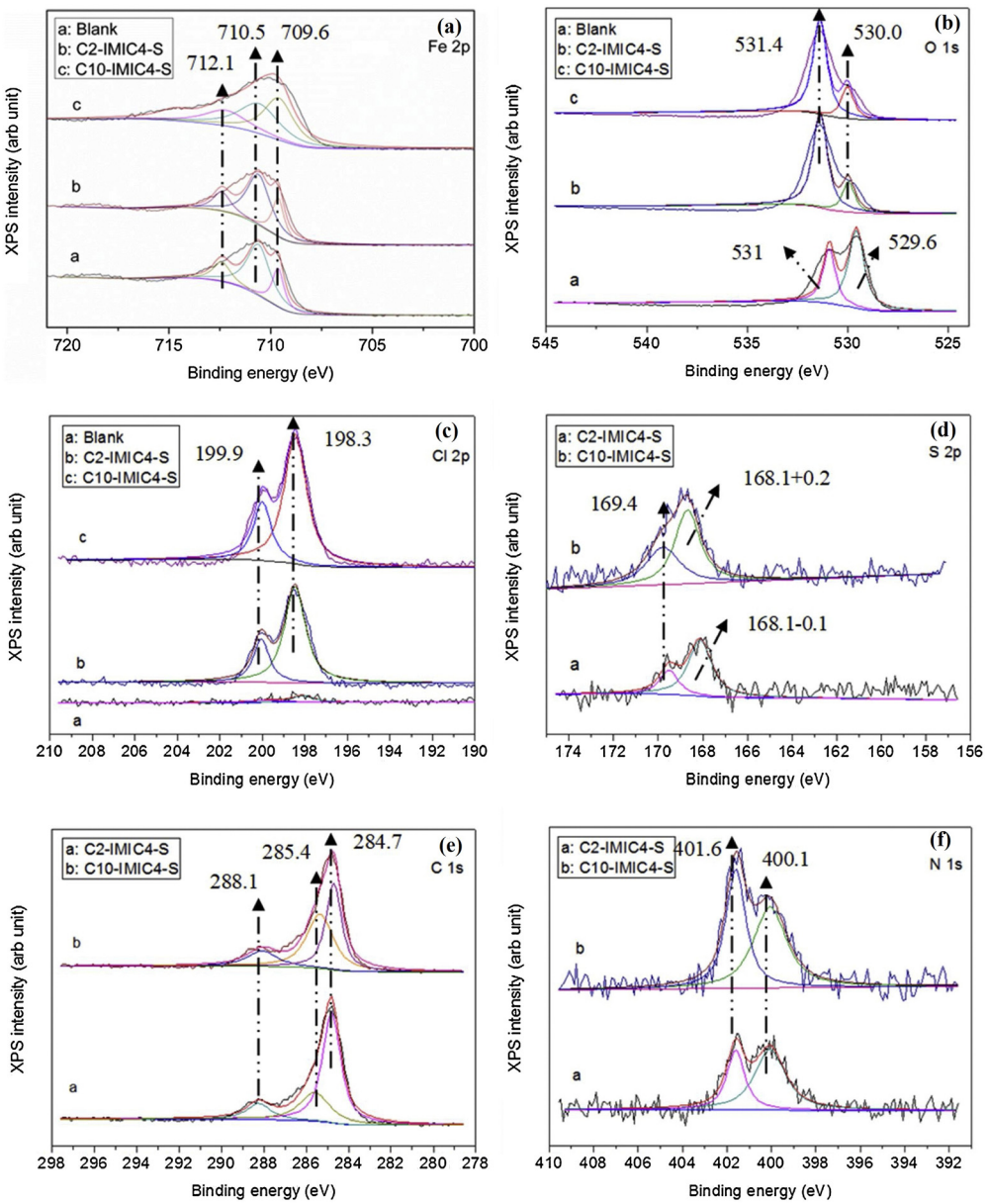

Fig. 12 XPS spectra for (a) Fe 2p, (b) O 1s, (c) Cl 2p, (d) S 2p, (e) C 1S, and (f) N 1s elements on the steel surface after 24 hours of immersion with and without 15 mM IL in 0.5 HCl solution [reprinted with permission from ref. 62, ©2019 Elsevier].

together, it can be inferred that the bonding of C and N species with the iron surface occurs in distinct ways, suggesting that the ImILs, along with the anion, can adhere to the steel surface as a whole. Hence, chemical adsorption is supported by XPS analysis.

It was found that the ImIL with a larger alkyl end triggered a more hydrophobic nature. In addition, the adsorptive nature of ImILs on the steel exterior results in the displacement of water molecules, which helps reduce the attack of hostile species. Consequently, a drop in double-layer capacitance was observed. Similarly, Haldhar *et al.* synthesized and characterized three ImILs, namely, 1-(2-methoxy-2-oxoe thyl)-3-methylimidazolium bromide (ILR1), 1-(2-ethoxy-2-oxoethyl)-3-methylimidazolium bromide (ILR2), and 1-(2-propoxy-2-oxoethyl)-3-methylimidazolium bromide (ILR3) with different chain lengths.[123] From the electrochemical and morphological analyses, the IE order was achieved as ILR1 < ILR2 < ILR3 for the protection of A1010 steel in 1 M HCl media. Even in the AFM study, the surface roughness of the mild steel immersed in 1 M HCl was found to be very high, while surface roughness started diminishing with the addition of ImILs. Notably, the surface roughness was significantly lower in the presence of ILR3 than in the presence of ILR1 and ILR2. The extended chain length of ILR3 was ascribed to its superior adsorption and strong corrosion inhibition capabilities compared to ILR2 and ILR1. Recently, Hajjaji *et al.* synthesized three new eco-friendly ImILs, namely, 3-benzyl-1-phenethyl-1*H*-imidazol-3-ium bromide [Met-IM$^+$, Br$^-$], 1,3-diphenethyl-1*H*-imidazol-3-ium bromide [Eth-IM$^+$, Br$^-$] and 1-phenethyl-3-(3-phenylpropyl)-1*H*-imidazol-3-ium bromide [Prop-IM$^+$, Br$^-$].[124] The anticorrosive effectiveness of these as-synthesized ILs in the presence of 37% HCl medium has been investigated thoroughly experimentally and theoretically. Electrochemical experimentations (EIS and PDP) were carried out in a 37% HCl medium in the absence and presence of various dosages of the ILs at various temperatures. The single semicircles obtained in the Nyquist plot indicated a charge transfer transition in the metal–electrolyte interface, *i.e.*, controlled corrosion was taking place. The depressed nature of the semicircles was obtained due to the surface roughness and the surface inhomogeneity. The data obtained from EIS were nicely fitted to the Randles equivalent circuit model. It was also observed that the R_{ct} values of the electrolyte solvent increased with the gradual addition of ILs. As the R_{ct} values are directly proportional to the adsorption capability of the compound, greater adsorption was attributed to [Prop-IMp, Br$^-$] because of its highest R_{ct} value. The order of IE of the ILs was [Prop-IM$^+$, Br$^-$] (97.3%) > [Eth-IM$^+$, Br$^-$] (95.7%) > [Met-IM$^+$, Br$^-$] (95.5%). These findings also indicate the stronger adsorption efficiency of [Prop-IM$^+$, Br$^-$] than the other two ILs. The adsorption nature was understood from the Arrhenius plot, *i.e.*, $\ln i_{corr}$ *vs.* $1000/T$ and $\ln (i_{corr}/T)$ *vs.* $1000/T$ plots. From these plots, the activation energy (E_a), activation entropy (ΔH_a) and activation enthalpy (ΔS_a) were successfully calculated from the slopes and intercepts. The high value of E_a indicates the physisorption of the ILs. The endothermic nature of the metal dissolution reaction process was established by the high positive values of ΔH_a.

Combined effects of chain length and aromatic ring. The combined effect of the two main regulating factors, *e.g.*, chain length and aromatic rings, was well explained by Zeng *et al.*[125] Their work revealed that the ImILs, namely, 1-propyl-3- methylimidazolium bromide ([PrMIm]Br), 1-aminopropyl-3-methylimidazolium bromide ([APMIm]Br) and 1,4-bis(3-methylimidazolium-1-yl) butane dibromide ([BMImB]Br_2) showed excellent corrosion inhibition effectiveness for the protection of mild steel in 0.5 M H_2SO_4 media. In the concentration range of 1 mM–7.5 mM at 303 K temperature, the IE of [APMIm]Br was found to be much superior to that of [BMIMB]Br_2 and [PrMIm]Br. This can be attributed to the presence of the –NH_2 group within the scaffold of [APMIm]Br, which is involved in electron donation from the non-bonding orbitals of N to the vacant d orbital of iron. Accordingly, [APMIm]Br creates a dense and well-ordered barrier film on a uniformly corroded mild steel surface. Notably, when the concentration is 10 mM, the charge transfer resistance rapidly increases for [BMIMB]Br_2. This outcome suggests that [BMIMB]Br_2 performs better in inhibiting corrosion at high concentrations than [APMIm]Br and [PrMIm]Br. This fact can be explained as a result of the chemisorption of [BMImB]Br_2 occurring more efficiently on the metal surface. Although there is an increase in the thermal movement between molecules as the temperature increases, the chemical bonds remain substantially stronger, leading to better corrosion prevention effectiveness. This chemisorption is mainly facilitated by the presence of both the additional carbon in the alkyl chain and the additional imidazolium ring.

Effects of synergism of constituent anion. To envisage the synergistic effect of the constituent ion of ImIL and the anions of corrosive media, a green ImIL, namely, 3-(4-fluorobenzyl)-1-methyl-1*H*-imidazol-3-ium bromide ([FBMIm]Br) was synthesized, and its protective performance against corrosion was investigated for steel surface in the presence of 0.5 M H_2SO_4.[126] It was found that 99.48% of IE was exhibited by 0.01 M IL at 298 K. Surface morphology study using SEM (a–d) and topographical study AFM (e–h) images of (a and e) the polished mild steel, (b and f) after immersion within 0.5 M H_2SO_4 without IL, (c and g) with 10^{-2} M [FBMIm]Br, and (d and h) with 10^{-5} M [FBMIm]Br as presented in Fig. 13 revealed the minimized degradation of surface and showed corrosion inhibition.

At 298 K, the morphological images of the pre- and post-corroded surfaces depict the surface protection of ImIL at a higher concentration (10^{-2} M) than that of a lower concentration (10^{-5} M). The surface roughness was also significantly low in the case of 10^{-2} M [FBMIm]Br/H_2SO_4 solution. The increase in corrosion retardation is based on two main factors: first, the adsorption of [FBMIm]Br on the metal surface and second, the synergistic effect induced by bromide ions. The negatively charged ions (SO_4^{2-}) of corrosive media compete with Br$^-$ ions in adsorption on metals. Thus, the formation of an insoluble cationic barrier of ImILs is intensely expedited.

Effects of synergism in the presence of external species. The addition of external ionic salt escalates the corrosion mitigation rate of ILs. A recent study revealed the protective nature of 1,1′ (1,4 phenylenebis(methylene))bis(3(carboxymethyl)1*H* imidazol 3 ium) chloride ImIL for carbon steel in the presence of 0.5 M HCl.[127] The synergistic effect of KI was

reported, and it was found that a 1 : 1 ratio of IL : KI showed 96.2% IE, wherein the same concentration of the ImIL exhibited 94.8% IE. The theoretical findings supported the experimental outcomes.

Similarly, other ILs, such as (*E*)-4-(4-nitrobenzylideneamino)benzoate (SNBB), 3,3′-diethylthiadicarbocyanine iodide (DI), and Thioflavin T (TT), are also preferable contenders to combat the adverse effects of corrosion.[128,129]

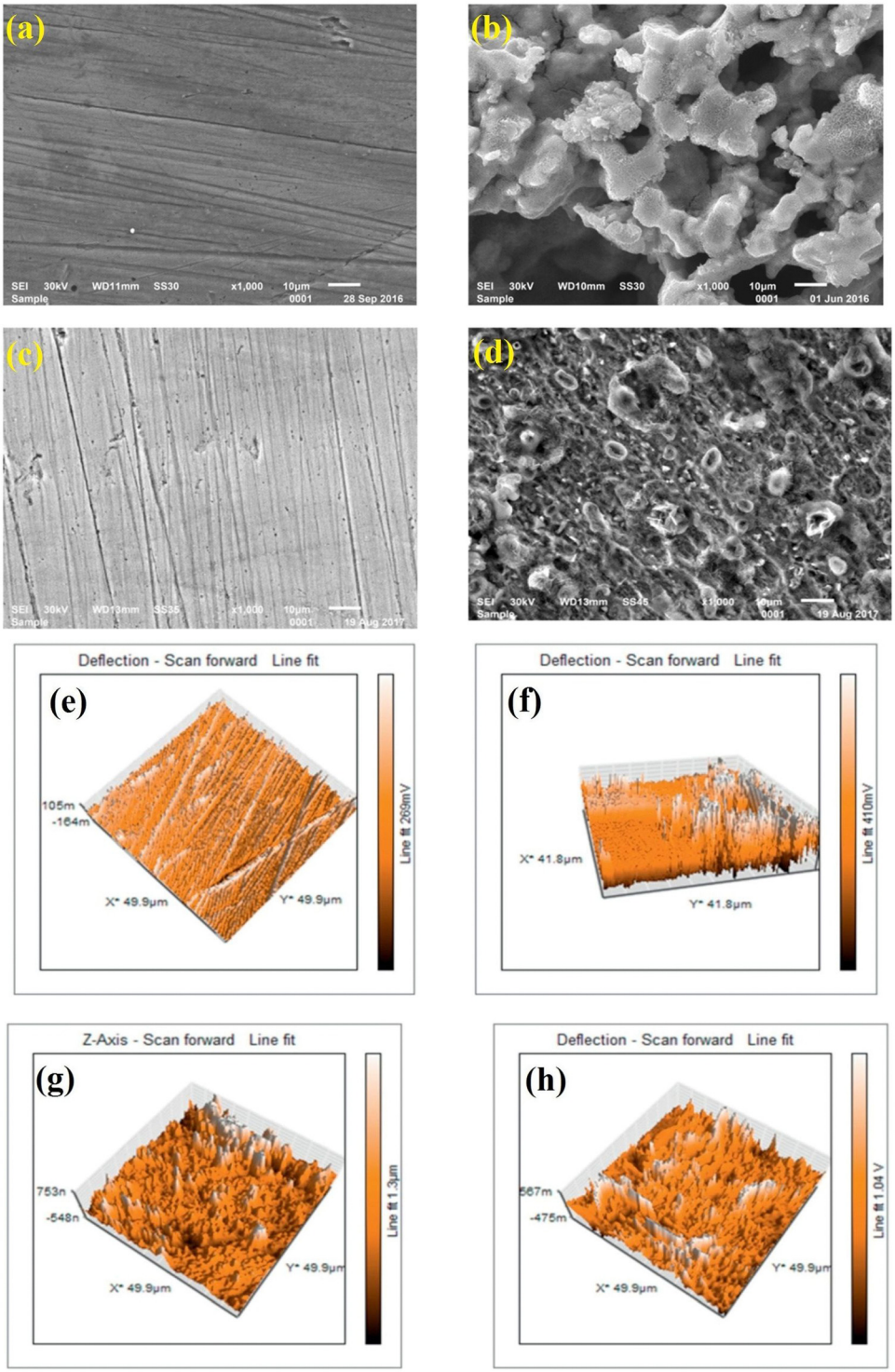

Fig. 13 SEM (a–d) and AFM (e–h) images of (a and e) the polished mild steel, (b and f) after immersion within 0.5 M H_2SO_4 without IL, (c and g) with 10^{-2} M [FBMIm]Br, and (d and h) with 10^{-5} M [FBMIm]Br. [Reprinted with permission from ref. 126, ©2019 Elsevier.]

Combined effects of constituent ions and alkyl chain length. Recent studies have shown seven ILs, namely, 1-ethyl-3-methylimidazolium hexafluorophosphate ($EMIMPF_6$), 1-methyl-3-pentyl-imidazolium hexafluorophosphate ($PenMIMPF_6$), and 1-methyl-3-octylimidazolium hexafluorophosphate ($OctMIMPF_6$), as corrosion inhibitors. Additionally, ILs with different anionic parts, for example, 1-methyl-1-octyl-pyrrolidinium hexafluorophosphate ($OctMpyrPF_6$), 1-methyl-1-octyl-pyrrolidinium thiocyanate (OctMpyrSCN), and 1-methyl-1-octyl-pyrrolidinium dicyanamide ($OctMpyrN(CN)_2$) with different constituent ions and alkyl chain lengths, could prevent mild steel from corroding in HCl environment.[130] Interestingly, when ILs with identical cations and anions were compared, the IL $OctMIMPF_6$, with its longest alkyl chain, provided the highest protective effectiveness. The creation of a compact film at the metal/electrolyte interface is facilitated by an increase in alkyl chain length, which leads to a remarkable increase in surface coverage and enhanced corrosion mitigation. Several prior studies have revealed comparable outcomes, demonstrating that an increase in alkyl chain length increases protection efficiency. However, herein, the interesting aspect is considering the cationic rings, *e.g.*, imidazolium, pyridinium, and pyrrolidinium. Imidazolium has a small net positive charge due to the delocalization of the positive charge on the nitrogen atom of the aromatic system. Additionally, the π-electron cloud of the imidazolium moiety can interact with the metal empty d orbital to get adsorbed onto the surface and hinder metallic dissolution. Pyridinium has a smaller molecular size than imidazolium and thus exhibits lower inhibitory efficacy. Conversely, the pyrrolidinium cation is a non-aromatic system and lacks delocalizable π-electrons, and its positive charge is concentrated on the N atom, resulting in a lower inhibitory efficacy than imidazolium. In contrast to ILs with the imidazolium cation, the strong positive charge on the N atom of the pyrrolidinium may exhibit some repulsive interactions with the positively charged steel surface in acidic electrolytic solutions, resulting in a reduction in its inhibition. The corrosion retardation applications of some ImIL-based inhibitors are tabulated in Table 3.

7. Cutting-edge computational approaches to assess the performance of the ILs in corrosion inhibition

Cutting-edge computational approaches are revolutionizing the field of corrosion inhibition. As computational power continues to increase and algorithms become more sophisticated, we can expect even more accurate and reliable predictions of the performance of ILs. This leads to the development of more effective and sustainable solutions for protecting metallic substances. Accordingly, the intriguing factors influencing the corrosion suppression performance of the ILs are discussed in light of computational modeling analysis. Undoubtedly, a thorough understanding of the inhibition process requires electronic-level insights between the interacting inhibitor molecules and metal substrates. Consequently, different computational approaches, such as density functional theory (DFT), density functional tight binding (DFTB), molecular dynamic (MD) and Monte Carlo (MC) simulations, for the congregation of results coming from different experimental outcomes can be an additional authenticate tool to strengthen the inferences. With these consequences, several researchers and scientists worldwide have also performed proper DFT studies, which strengthen the observations that come from experimental observations. However, before going for modelling, it is always an imperative criterion to consider a system wherein the electrons reside, and its quantitative approach is very crucial. In this context, both DFT and DFTB calculations are important. Over the last few decades, research on corrosion inhibition mechanisms has effectively utilized first-principles calculations based on the fundamental equations of quantum theory, which explain the behaviour of electrons, atoms, and molecules. DFT has been utilized to understand electronic or quantum chemical parameters, while DFTB can do so in a more directive manner.[131,132]

Several regulating factors, such as chain lengths, functional groups, and aromaticity, affecting corrosion inhibition effectiveness have been well explained through several efficient computational aspects.[131,133,134] In addition, the complicacy of the corrosion inhibition mechanism has driven the adaptation of the quantitative structure activity relationship (QSAR) model. QSAR analysis increasingly influences the electronic nature of the molecules described by wave functions. Quantum descriptors incorporating both electronic and molecular information are preferred for the development of the QSAR model. These descriptors provide predictions regarding the theoretical IE of the studied system.

7.1. Insight through the first principle calculation

DFT provides a powerful framework for simulating the interactions between ILs and metal surfaces at the atomic level. DFT analysis allows for the evaluation of the adsorption energy (E_{ads}) of ILs on metal surfaces. This information is crucial for understanding the strength of the bond between the IL and the metal, which directly impacts the effectiveness of corrosion inhibition. By analyzing the charge density distribution and the interaction between the orbitals of the IL and the metal, researchers can gain insights into the mechanism of corrosion inhibition. By computationally screening large numbers of ILs, researchers can identify promising candidates for further experimental evaluation.[106,135]

Computational studies based on DFT are commonly employed to illustrate the donor–acceptor nature of the two interacting species.[136–139] Various important electronic parameters, such as the highest occupied molecular orbital (HOMO), lowest unoccupied molecular orbitals (LUMO), and associated energies (E_{HOMO} and E_{LUMO}), their energy difference (ΔE), electronegativity, electron affinity, and the fraction of electrons transferred between the inhibitor and metal, are determined from DFT calculations. The electronic distribution in the frontier molecular orbitals (FMOs *i.e.*, HOMO and LUMO) is admirably an important aspect in understanding the electron-donating or accepting sites. Generally, the donor property of the inhibitor increases with an increase in the

Table 3 ImIL as an anticorrosive additive for the protection of steel surface from a corrosive environment

Sl. no.	Ionic liquid (Structure/IUPAC name)	Metal surface and medium	Adsorption mechanism	Isotherm model	Highlights	Ref.
1	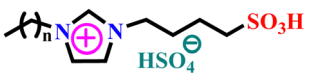 n=1: 1-(4-sulfonic acid) butyl-3-ethylimidazolium hydrogen sulfate (C2-IMIC4-S) and n=10: 1-(4-sulfonic acid) butyl-3-decylimidazolium hydrogen sulfate (C10-IMIC4-S)	Carbon steel/0.5 M HCl	Physisorption, chemisorption and mixed	Langmuir	(i) IE: 80.8% for C2-IMIC4-S and 97.9% C10-IMIC4-S@ 15 mM and 25 °C (ii) The larger chain length of C10-IMIC4-S is responsible for its better adsorption on metals	62
2	 1-(2-carboxylic acid) ethyl-3-methylimidazolium hydrogen sulfate ($[(CH_2)COOHMIm][HSO_4]$) 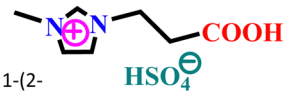 1-(2-carboxylic acid) ethyl-3-methylimidazolium hydrogen sulfate ($[(CH_2)_2COOHMIm][HSO_4]$) 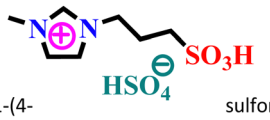 1-(4-sulfonic acid) propyl-3-methylimidazolium hydrogen sulfate ($[(CH_2)_3SO_3HMIm][HSO_4]$)	Mild steel/ 0.5 M HCl	Both physisorption and chemisorption	Langmuir	(i) IE: 75.8% for $[(CH_2)COOHMIm][HSO_4]$, 89.5% for $[(CH_2)_2COOHMIm][HSO_4]$ and 93.0% for $[(CH_2)_3COOHMIm][HSO_4]$@10 mM and 298 K (ii) The functional groups and the additional alkyl group within the cationic part increased the inhibitory process of the $[(CH_2)_3SO_3HMIm][HSO_4]$ IL	120
3	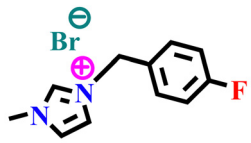 3-(4-Fluorobenzyl)-1-methyl-1H-imidazol-3-ium bromide ([FBMIm]Br)	Mild steel-/ 0.5 M H_2SO_4	Physical and chemical adsorption	Langmuir	(i) IE: 98.90% @0.01 M and 298 K (ii) The synergistic effect of bromide (Br^-) results in a better protective nature of this IL	126
4	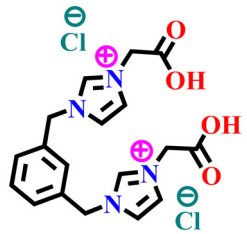 1,1′-(1,4-phenylenebis(methylene))bis(3-(carboxymethyl)-1H-imidazol-3-ium) chloride	Carbon steel/0.5 M HCl	Predominant chemisorption	Langmuir	(i) IE: 94.8% for 1 mM IL and 96.2% for IL : KI of 1 : 1 (ii) IL and KI inhibited the corrosion process through strong synergism	127
5	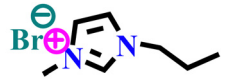 1-propyl-3-methylimidazolium bromide ([PrMIm]Br)	Mild steel/ 0.5 M H_2SO_4	Physicochemical adsorption	Langmuir	(i) IE: 60.4% for [PrMIm]Br, 86.4% [APMIm]Br and 91.0% for $[BMImB]Br_2$@10 mM and 303 K	125

Table 3 (*continued*)

Sl. no.	Ionic liquid (Structure/IUPAC name)	Metal surface and medium	Adsorption mechanism	Isotherm model	Highlights	Ref.
	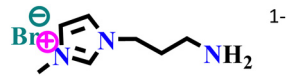 1-aminopropyl-3-methylimidazolium bromide ([APMIm]Br)					
	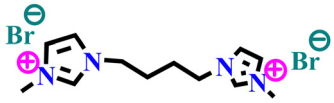 1,4-bis(3-methylimidazolium-1-yl)butane dibromide ([BMImB]Br_2				(ii) An increase in corrosion IE was triggered by an increase in the chain length within the cationic part	
	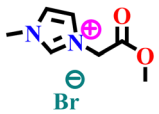 1-(2-methoxy-2-oxoethyl)-3-methylimidazolium bromide(ILR1)				(i) IE: 84.50% for ILR1, 92.95% for ILR2 and 95.77 for ILR3@1 mM and 298 K	
6	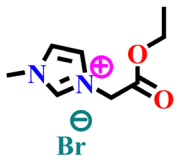 1-(2-ethoxy-2-oxoethyl)-3-methylimidazolium bromide(ILR2),	A1010 steel/1 M HCl	Physisorption and chemisorption	Langmuir	(ii) Increased IE resulted in increased surface coverage with elongation of the aliphatic chain length	123
	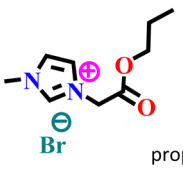 1-(2-propoxy-2-oxoethyl)-3-methylimidazolium bromide(ILR3)					
	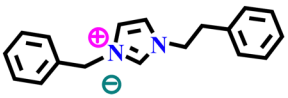 3-benzyl-1-phenethyl-1H-imidazol-3-ium bromide [Met-IM^+, Br^-]				(i) IE: 95.5% for [Prop-IM^+, Br^-], 95.7% for [Eth-IM^+, Br^-] and 97.3% for [Met-IM^+, Br^-]@10^{-3} M	
7	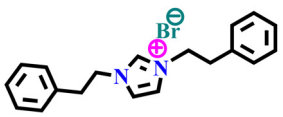 1,3-diphenethyl-1H-imidazol-3-ium bromide [Eth-IM^+, Br^-]	Mild steel/ 37% HCl	Predominantly chemisorption	Langmuir	(ii) An increase in the carbon number within the aliphatic moiety facilitated better adsorption of the IL, which was further associated with the +I effects of the alkyl groups	124
	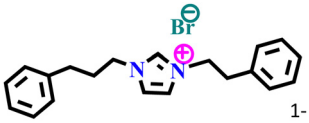 1-phenethyl-3-(3-phenylpropyl)-1H-imidazol-3-ium bromide [Prop-IM^+, Br^-]					

Table 3 (*continued*)

Sl. no.	Ionic liquid (Structure/IUPAC name)	Metal surface and medium	Adsorption mechanism	Isotherm model	Highlights	Ref.
	 1-vinyl-3- methylimidazolium iodide ([VMIM]I)				(i) IE: 96% for [VMIM]I, 97% for [VPIM]I and 99.4% [VBIM]I@5 mM and 298 K (ii) An increase in IE was associated with an increase in alkyl chain length	
8	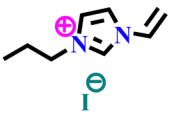 1-vinyl-3-proplylimidazolium iodide ([VPIM]I)	X70 steel/ 0.5 M H_2SO_4	Physisorption and chemisorption	Langmuir		122
	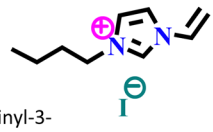 1-vinyl-3-butylimidazolium iodide ([VBIM]I)					
	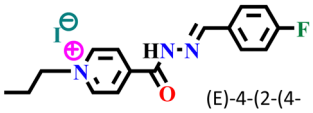 (E)-4-(2-(4-fluorobenzylidene)hydrazinecarbonyl)-1-propylpyridin-1-ium iodide [Ipyr-C_3H_7]				(i) IE: 88.6% for Ipyr-C_3H_7, 87.8% for Ipyr-C_5H_{11}@10^{-3} M and 298 K	
9	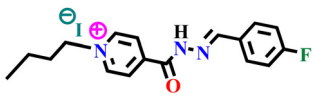 (E)-4-(2-(4-fluorobenzylidene)hydrazinecarbonyl)-1-pentylpyridin-1-ium iodide [Ipyr-C_5H_{11}]	Mild steel/ 1 M HCl	Both physisorption and chemisorption	Langmuir	(ii) These ILs showed better protective ability with varying temperature ranges and different immersion times (iii) An increase in IE was observed for the IL with the alkyl group of four C, but after more increase in the alkyl group, IE decreased because of agglomeration	104

HOMO value. In a recent work based on cetylpyridinium picrate (CPP) IL, it is observed that the electron cloud is mainly located on the anionic part of the protonated and neutral IL, as depicted in Fig. 14(a) and (b).[15] This suggests that the anionic part is mainly responsible for the electron donation or acceptance properties. It is worth mentioning that the electronic orbitals strongly participate in the adsorption process. In the case of 1-octyl-3-methylimidazolium L-prolinate ([Omim]Lpro) ImIL, the cationic part is mainly responsible for chemisorption because of its lower ΔE value.[140]

From Fig. 14(c) and (d), it is evident that the distribution of HOMO in both neutral and protonated forms of 1-decyl-3-methylimidazolium chloride (DMIC) is centred on the chloride ion. The LUMO is concentrated on the cationic portions of the imidazoline rings of the neutral and protonated forms, that is the anionic counterpart takes part in electron donation during the adsorption process. Additionally, the cationic imidazolium part is involved in the electron acceptance process. Higher E_{HOMO}, lower E_{LUMO} and lower ΔE values in the case of neutral form than the protonated form of the ImIL suggest better adherence of the neutral form on the P110 steel when immersed in 15% HCl medium. To understand the effect of functional group, the HOMO–LUMO plots of [(CH_2)COOHMIm][HSO_4], [$(CH_2)_2$COOHMIm][HSO_4] and [$(CH_2)_3SO_3$HMIm][HSO_4] play a vital role (*vide*, Fig. 14(e), (f) and (g)). Particularly, the partial imidazole ring and –COOH group contain the majority of the HOMO of the cation of [(CH_2)COOHMIm][HSO_4]. However, HOMO is mostly found in the –COOH group for [$(CH_2)_2$COOHMIm][HSO_4]. In contrast, the –SO_3H group is the central point of the HOMO of [$(CH_2)_3SO_3$HMIm][HSO_4]. Therefore, functional groups play a principal role in adsorption through electron donation.

Additionally, in several recent studies, the identification of local reactive sites within the inhibitor has been aided by the analysis of Fukui indices (FIs).[14,17,42] Herein, f_K^+ and f_K^-, are designated as the corresponding Fukui functions that induce the respective sites to react *via* nucleophilic and electrophilic reaction pathways, respectively. In a recent study, FI analysis was executed to unveil the location of the reactive atoms within the L-alanine methyl ester nitrate (LAlaC$_1$NO$_3$) AILs.[42] It was

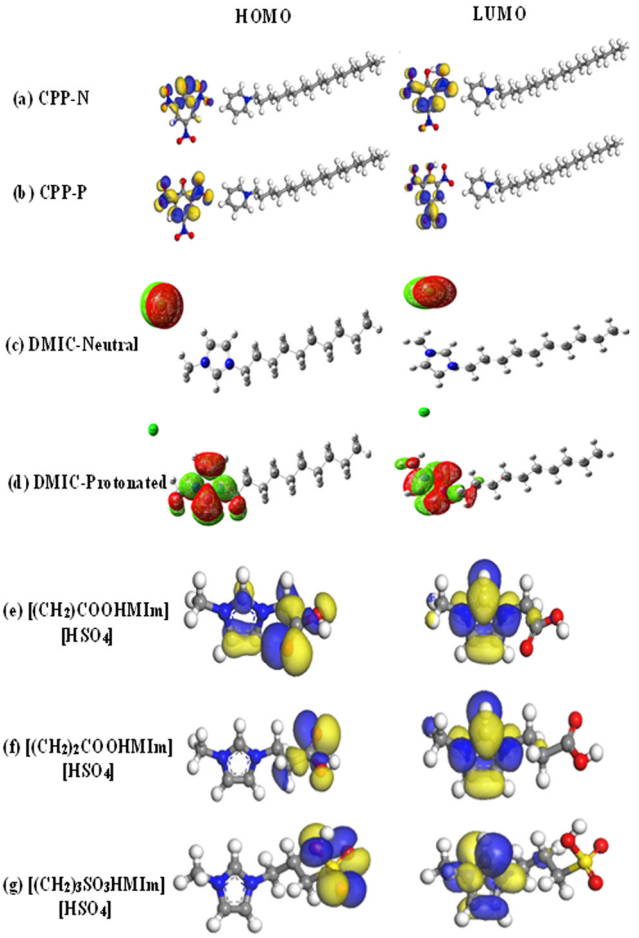

Fig. 14 Pictorial representation of the HOMO and LUMO orbitals of (a) CPP-N, (b) CPP-P, (c) DMIC-Neutral, (d) DMIC-Protonated, (e) [(CH_2)COOHMIm] [HSO_4], (f) [$(CH_2)_2$COOHMIm] [HSO_4] and (g) [$(CH_2)_3SO_3$HMIm] [HSO_4] (red colour: oxygen, grey colour: carbon, blue colour: nitrogen, white colour: hydrogen, yellow colour: sulphur). [Reprinted with permission from ref. 15, ©2023 Elsevier, ref. 39, ©2021 Elsevier, and ref. 115, ©2020 Elsevier.]

observed that the nucleophilic attacks were more facilitated on the anionic parts of the IL as the f_K^+ values were exceptionally high on those sites.

7.2. Insight through DFTB

Although the DFT approach is the most popular and widely used *ab initio* technique, this first principal calculation is unable to provide atomistic details regarding the inhibition mechanism of large inhibitors. Accordingly, theoretical approaches to address the adsorption issue of large-sized inhibitors must be found to gain a deeper understanding of the mechanistic roadmap of the inhibition process. Researchers have realized that studying the adsorption phenomena of organic macromolecules on metal surfaces may be possible using this quasi-empirical DFTB method. DFTB consolidates the tight binding technique with the higher accuracy and efficiency of the *ab initio* DFT approach.[141]

In this regard, an investigation of the adsorption of 1-butylpyridinium cations onto the Fe(110) plane was carried out using the DFTB study.[35] It was observed that the electron-rich benzene moiety of the corrosion inhibitors 1-butylpyridinium chloride (BPC) and 1-butylpyridinium hexafluorophospate (BPH) allowed their cationic components to be adsorbed horizontally on the Fe(110) plane *vide*, as depicted in Fig. 15(a) and (b). The 1-butylpyridinium moiety of the BPC and BPH ILs has a considerable adsorption capability, as indicated by the extremely negative magnitude of E_{ads}. Fig. 15(c) depicts the plotted charge density differences triggered by the adsorption of 1-butylpyridinium cation on the Fe(110) surface. Fig. 15(c) demonstrates that when the 1-butylpyridinium moiety comes closer to the iron surface atoms, the adsorption of the 1-butylpyridinium moiety occurs. The contact and electron sharing between the 1-butylpyridinium moiety and the iron surface atom resulted in the blue area displaying electron-rich sites and the red region displaying electron-deficient sites.

Accordingly, it could be concluded that the 1-butylpyridinium moiety appears to promote the adsorption of the ILs. To shed further light on the nature of the interactions, the projected density of states (PDOS) to the ILs and the Fe atoms that bond to the respective cationic moiety were plotted. Fig. 15(d) and (e) illustrate the PDOS plot of the 1-butylpyridinium moiety and iron surface before adsorption. Fig. 15(f) illustrates the PDOS plot that emerged owing to the interactions of the 1-butylpyridinium moiety on the Fe(110) surface. Notably, the vertical dotted line indicates that the Fermi energy level was set to zero. The inhibitor peaks are sharper prior to adsorption, but these peaks start broadening with adsorption, indicating robust adsorption between the cationic part of the PyIL and the Fe surface. Similarly, compared to the PDOS peaks for Fe before adsorption, the Fe peaks after adsorption are not as sharp before adsorption. Accordingly, from the PDOS analysis, it can be inferred that the presence of an aromatic moiety enhanced the adherence tendency of the ILs onto the targeted metal exterior.

7.3. Insight through the light of MD simulation

In the current scenario, MD simulation has attracted superior attention in the scientific community owing to its simpler, more affordable technique and capability to produce molecular insights.[142] In other words, the key objective of MD simulation is to gather molecular-level information regarding the structure and dynamics of a classical main-body system under equilibrium, as governed by the classical Newtonian mechanism.[143] MD simulation can assist in determining the macroscopic parameters of a system, such as the coordination number, radial distribution function (RDF), average potential energy, diffusion, and density of systems containing a significant number of molecules.[142,144] An analysis of MD simulations can reveal the details regarding the orientation of molecules on metal surfaces, as well as the interaction energy (E_{int}) and binding energy (E_{bind}). MD simulation is considerably utilised in the vicinity of corrosion inhibition by ILs. If the total energy of the simulated system, the energy of the IL and the energy of metal with the simulated corrosive electrolytic solution are E_T, E_{IL} and E_{M+E} respectively, then the E_{int} and E_{bind} are as follows (*vide* eqn (1) and (2)):[15,145–149]

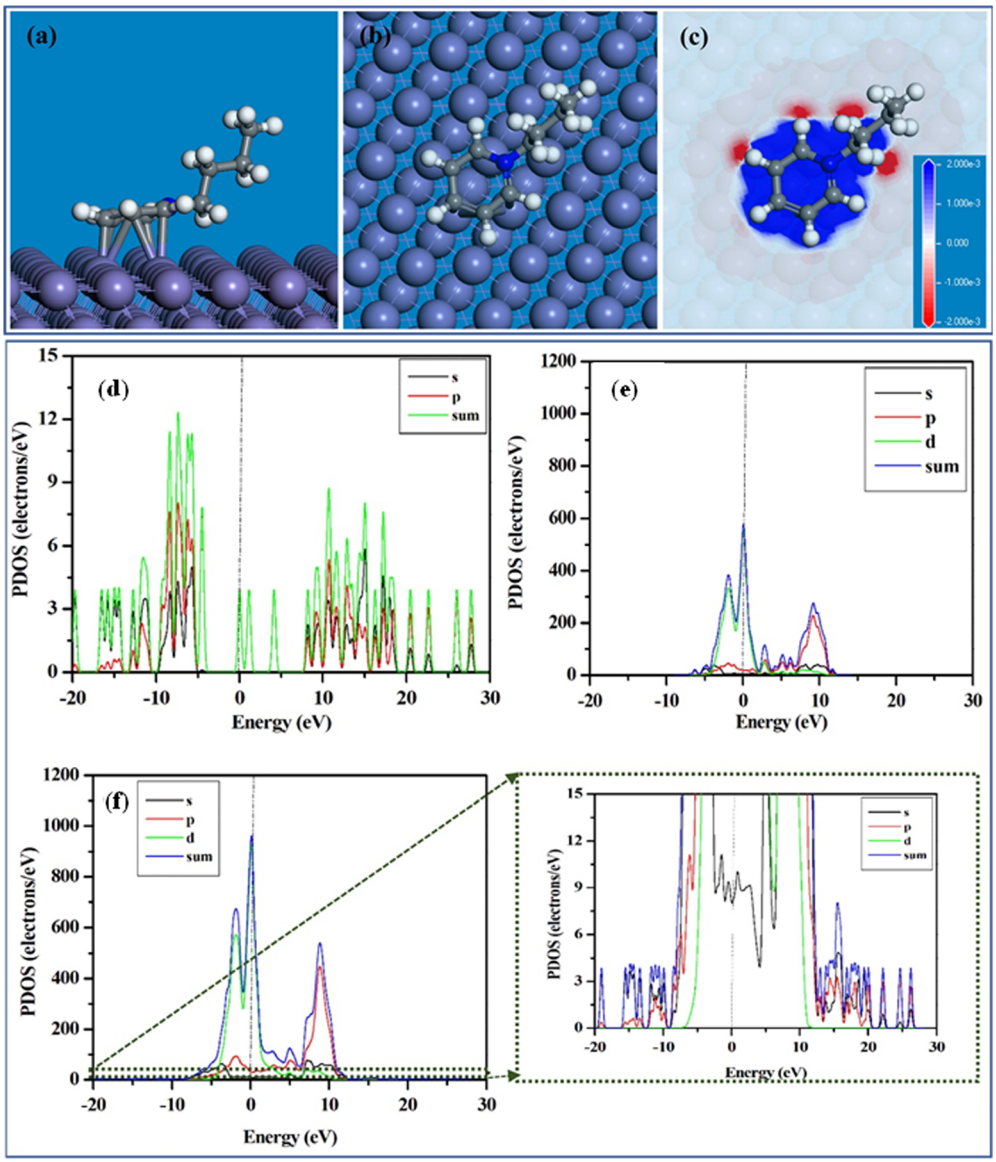

Fig. 15 (a) Side view, (b) top view, (c) charge density difference plot of the equilibrium adsorption configuration of 1-butylpyridinium cation on Fe(110) surface; partial density of states (PDOS) of (d) 1-butylpyridinium cation, (e) iron surface and (c) 1-butylpyridinium cation after adsorption on Fe(110) surface. [Reprinted with permission from ref. 35, ©2023 Elsevier.]

$$E_{int} = E_T - (E_{M+E} + E_{IL}) \quad (1)$$

$$E_{bind} = -E_{int} \quad (2)$$

The higher the negative value of E_{int}, the better the interaction between the IL and the metal plane. From the orientation of the ILs, it is clear which structural part of the IL is actually taking part in adsorption and how. Accordingly, the effect of the regulating factors can be explained satisfactorily. Recent works based on MD simulation have been discussed, *vide infra*. Recently, in 2021, Singh *et al.* reported the anticorrosive behaviour of three commercially available PiILs, namely, IL-1, IL-2, and IL-3, for retarding the corrosion rate of Q235 steel in the presence of 1 N HCl.[100] In the MD simulation study, the three ILs with different chain lengths were separately allowed to get adsorbed on the Fe(110) plane in the presence of 150 H_2O, 15 H_3O^+ and 15 Cl^- ions. The equilibrium adsorption configurations revealed the flat horizontal orientation of the ILs, *vide* Fig. 16.

The E_{int} values for IL-1, IL-2, and IL-3 were found to be -660.56 kJ mol^{-1}, -710.46 kJ mol^{-1}, and -906.56 kJ mol^{-1}, respectively. This outcome implies that the ILs interact in the sequence IL-2 > IL-1 > IL-3, validating the experimental outcomes. The effect of alkyl chain length was lucidly elaborated through the MD simulation. From the E_{int} values, it was observed that IL-2 and IL-3 have a higher interaction capability with the metal, which may be attributed to the presence of longer alkyl chains. However, IL-3 possesses a better interacting capability than that of IL-2. This fact can be explained by the presence of the larger anionic moiety within IL-3, which facilitates better surface coverage.

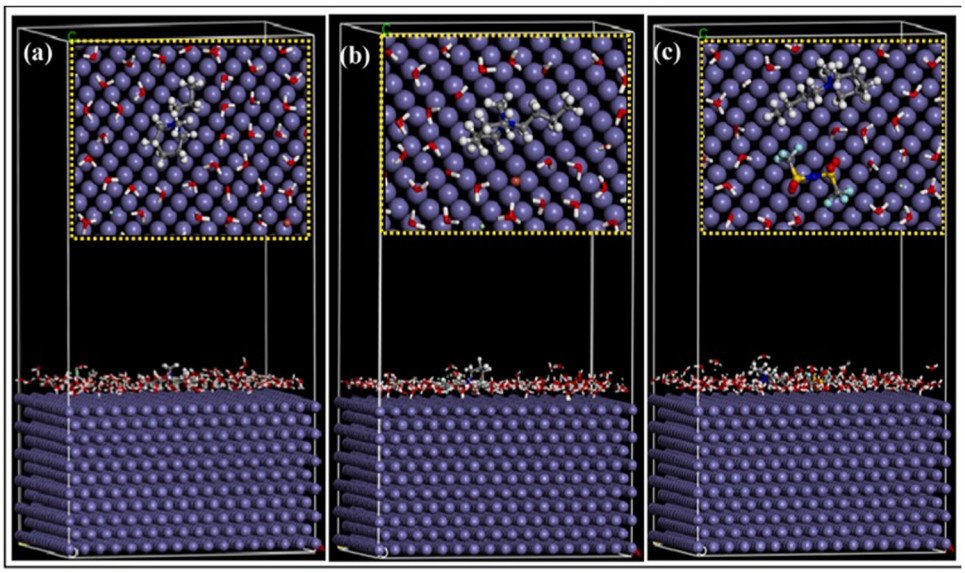

Fig. 16 Side view of the optimized adsorption configuration of (a) IL-1; (b) IL-2 and (c) IL-3 on the Fe(110) plane in a simulated acid medium (*i.e.*, in the presence of 150 H_2O, 15H_3O^+ and 15Cl^-) obtained from MD simulation (inset: top view). [Reprinted with permission from ref. 100, ©2021 Elsevier.]

To achieve the effect of the aromatic moiety on the anti-corrosive nature of AmILs, an MD simulation study accompanied by an RDF analysis was performed.[97] In the MD simulation study, the three AmILs were allowed to get adsorbed on the Fe(110) surface in the presence of H_2O, H_3O^+ and Cl^- ions. As per the equilibrium adsorption model, when the ILs bind to the Fe(110) crystal surface, it does not allow for the presence of any H_2O, H_3O^+ and Cl^- ions between the ILs and the metal exterior. This indicates that the ILs replace any pre-adsorbed solvent or other ionic species in the electrolyte medium and form a robust shielding layer in the metal electrolyte interface. Similarly, the adsorption patterns of the $[Ch]^+$ cations of ILs are almost identical on the Fe(110) surface. Therefore, the discrepancy in corrosion mitigation effectiveness can be ascribed primarily to the alterations in anions. The anionic parts of the AmILs, including the benzene ring portion, amino group, and indole moiety, orient themselves in a parallel fashion on the Fe surface, while the carboxyl group exerts itself outward. The carboxyl group aids in enhancing the surface coverage and facilitates strong bonding with the underlying surface, leading to more stable adsorption. Based on the results of the MD simulations, it can be concluded that the pre-occupied solvent or other corrosive species can be replaced by corrosion inhibitors. The effective estimation of bond length can be achieved by applying RDF, denoted by $g(r)$.[99,150–153] It is possible to extract insights into the interaction between the simulated metal surface and the AmILs by examining the peaks. Chemisorption of the ILs was evidenced by the appearance of the first peak within the range of 1–3.5 Å, while physisorption was confirmed by the appearance of a peak greater than 3.5 Å. These outcomes indicated that chemisorption is the predominant factor during the adsorption of the AmILs. The corrosion inhibition is schematically presented in Fig. 17.[99]

The metal surface can be significantly safeguarded against corrosion by acidic solutions when choline amino acid AmIL corrosion inhibitors are adsorbed on it in a mixed manner, *i.e.*, physisorption and chemisorption. It is evident from process-1 in Fig. 17(a) that there is a diminishing tendency of electrochemical reactions (cathodic and anodic), resulting in a drop in

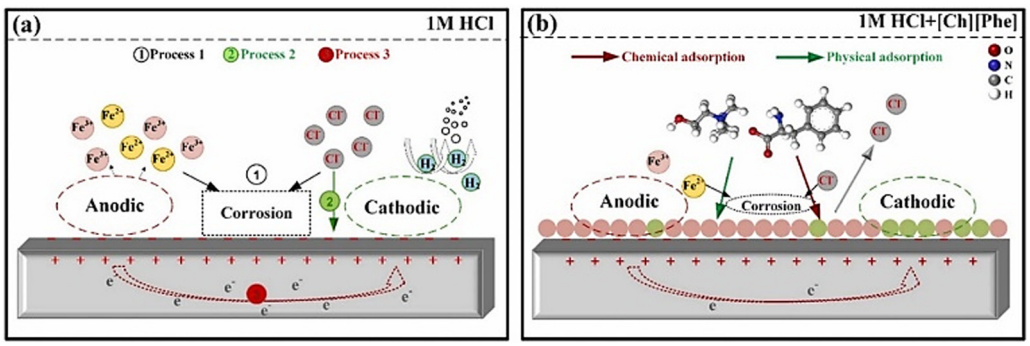

Fig. 17 Schematic representation of the (a) corrosion mechanism of mild steel in the presence of 1 M HCl and (b) corrosion inhibition mechanism of mild steel in the presence of [Ch][Phe] in 1 M HCl solution. [Reprinted with permission from ref. 99, ©2023 Elsevier.]

electron transfer within the metal surface, *vide* process 3. Moreover, the adsorption of the AmILs leads to the displacement of Cl^- ions pre-adsorbed on the mild steel exterior, that is desorption of Cl^- takes place. As depicted in Fig. 17(b), it is clearly visible that the adsorbed Cl^- anions attract cations of the AmILs through strong electrostatic interaction. Consequently, the physisorption of AmILs takes place, and the hydrogen generation reaction in cathodic sites is reduced. However, heteroatoms, such as N and O, and unsaturated bonds participate in donor–acceptor interactions with the molecular orbitals of the metal, which facilitates chemisorption of the ILs. Both the theoretical analysis and experimental findings yield a similar order of IE: [Ch][Phe] > [Ch][Trp] > [Ch][Tyr].[104] RDF analysis is employed to identify the type of interaction between the adsorbate and the adsorbent, whether it is physisorption, chemisorption, or both. Fig. 18 illustrates that the first peak values for each bond length of Ipyr-C_3H_7 and Ipyr-C_5H_{11} adsorption on the Fe(110) surface at a simulated temperature of 298 K suggest chemisorption interaction for Fe–N9 (2.77 Å), Fe–N10 (2.86 Å), and Fe–N17 (2.79 Å) bond lengths.

Organic corrosion inhibitor molecules typically work through adsorption on a specified metal surface. The presence of an aromatic ring, azomethine linkage, and –NH– moiety present within the IL scaffold facilitates the chemisorption of the IL on the targeted metal substrate. These aforementioned factors allow the electron cloud to be shared with the empty orbitals of the metal.

Cao *et al.* synthesized two task-specific Brønsted acid ILs (BAILs), namely, 1-(4-sulfonic acid) butyl-3-ethyl imidazolium hydrogen sulfate and 1-(4-sulfonic acid) butyl-3-decyl imidazolium hydrogen sulfate, designated as C2-IMIC4-S and C10-IMIC4-S,[62] respectively. Molecular orbital theory and MD simulation studies were conducted to corroborate the experimental observations. The equilibrium configuration after the adsorption of the cations of C2-IMIC4-S and C10-IMIC4-S on the Fe(001) surface in vacuum and the aqueous phase was considered. It can be observed that the cations of both ILs are projected in a parallel fashion, which is advantageous for achieving high coverage and effective protection against corrosion. The orientation of the imidazole ring of both the C2-IMIC4-S and C10-IMIC4-S molecules is parallel to the simulated metal surface, promoting high surface coverage and efficient IE. The E_{ads} of the cations on the Fe(001) surface in the presence of solution followed the order of C10-IMIC4-S (-1110.74 kJ mol^{-1}) < C2-IMIC4-S (-237.30 kJ mol^{-1}). A more negative E_{int} or a more positive E_{bind} value indicates a higher stability of the adsorption of IL cations on the Fe(001) surface, which could lead to superior inhibition performance.

Similarly, the effects of alkyl chain length were explored for three ImILs, namely, 3-benzyl-1-phenethyl-1*H*-imidazol-3-ium bromide [Met-IM$^+$, Br$^-$], 1,3-diphenethyl-1*H*-imidazol-3-ium bromide [Eth-IM$^+$, Br$^-$] and 1-phenethyl-3-(3-phenylpropyl)-1*H*-imidazol-3-ium bromide [Prop-IM$^+$, Br$^-$] through MD simulation.[124] The ILs were horizontally oriented onto the Fe(110) surface. The computed adsorption energies were found to be -197.151, -187.249 and -182.243 kcal mol^{-1} for [Prop-IM$^+$, Br$^-$], [Eth-IM$^+$, Br$^-$], [Met-IM$^+$, Br$^-$], respectively. The greater the E_{ads}, the greater the binding of the species to the

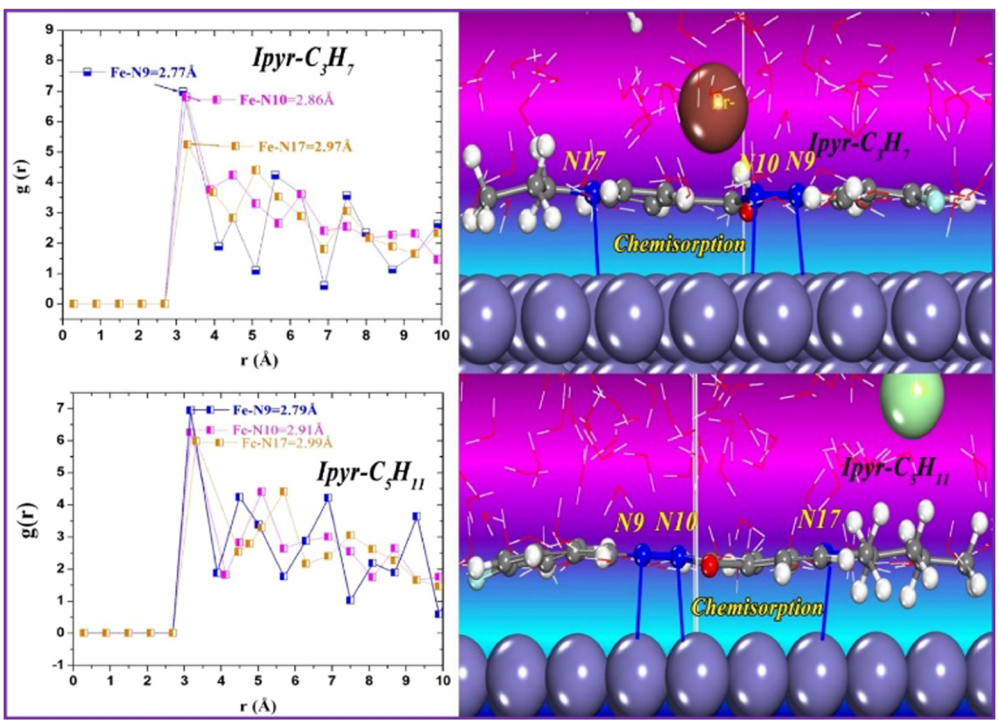

Fig. 18 RDF analysis of adsorbed Ipyr-C3H7 and Ipyr-C5H11 on Fe(110) surface in a simulated acid medium at 298 K temperature obtained from MD simulation. [Reprinted with permission from ref. 104, ©2021 Elsevier.]

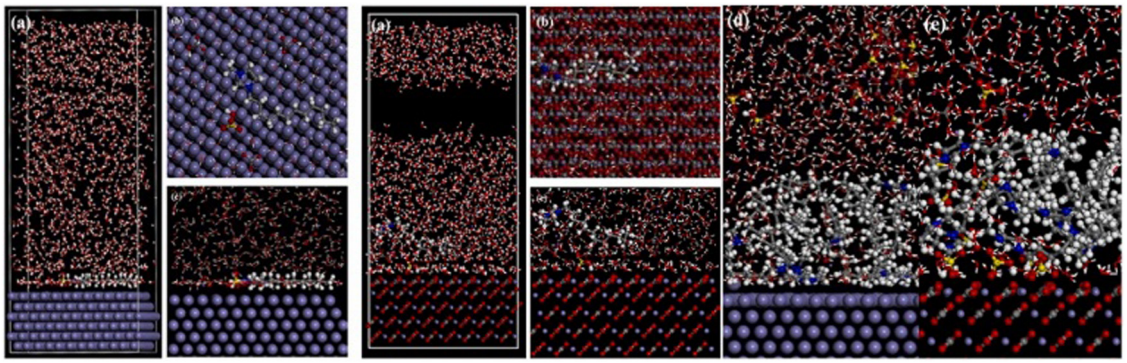

Fig. 19 Optimized adsorption configuration of the adsorption of one DMIMHS on Fe(110) (first column) and $FeCO_3$(104) (middle two columns): (a) overall view, (b) top view and (c) side view; optimized adsorption configuration of nine DMIMHS on (d) Fe(110) and (e) $FeCO_3$(104). [Reprinted with permission from ref. 119, ©2022 Elsevier.]

surface. Accordingly, the MD simulation study also supported the idea that [Prop-IM^+, Br^-] has a better adsorptive capability. Henceforth, it acted as a better corrosion inhibitor among the three ILs. In this case, the strong adsorption involved may be attributed to either physisorption, chemisorption or both. The positively charged species is responsible for physisorption because it is electrostatically attached to the Cl^- ions on the metal surface. As reported, the ILs form coordinate bonds *via* the sharing of electrons from the filled orbitals of heteroatoms to the vacant d-orbitals of Fe metal, which facilitates chemisorption. Additionally, the π-electrons situated in the aromatic rings also take part in the donor–acceptor-like interaction, resulting in back donation, also known as retro-donation. The large surface area of the ILs helps cover the surface of the underlying metal; thus, the metal is protected from an aggressive environment. In another study, the ImIL, namely, DMIMHS, was allowed to get adsorbed on Fe(110) and $FeCO_3$(104) at the molecular level to understand the adsorption sites along with the adsorption mechanism of the ImIL on a metal substrate.[119] The top and side views of the adsorption of DMIMHS are presented on Fe(110) and $FeCO_3$(104) surfaces, as depicted in the first two columns of Fig. 19(a), (b) and (c). The equilibrium adsorption of nine DMIMHS ILs on the Fe(110) and $FeCO_3$(104) surfaces is depicted in the middle two columns of Fig. 19(a), (b) and (c). It was found that the DMIMHS ILs are adsorbed horizontally on the Fe(110) surface, but in the case of the adsorption on the $FeCO_3$(104) plane, the anionic part of DMIMHS, that is HSO_4^-, is adsorbed on the surface, and the aromatic imidazole moiety exerts itself in the outwards of the surface. The calculated binding energy values for the adsorption of DMIMHS were found to be 280.01 kcal mol^{-1} and 35.21 kcal mol^{-1} for the Fe(110) and $FeCO_3$(104) surfaces, respectively. These results suggest a better interaction of IL, leading to efficient adsorption and better protection of the iron surface. Based on the experimental and theoretical findings, a probable interaction mechanism is proposed for the protective mechanism of the IL on the targeted surfaces, *vide* Fig. 20.

From DFT analysis, it was confirmed that the HOMO orbital electron density is mainly situated in the anionic part, that is HSO_4^-, while the electron density of LUMO is mainly concentrated in the imidazole rings. In the presence of the brine solution, DMIMHS IL is dissociated into two ionic parts: the cationic part is the imidazolium moiety and the anionic part is the HSO_4^-. Accordingly, in the presence of NaCl medium, the HSO_4^- parts are involved in electron donation to the vacant d orbitals of Fe, resulting in chemisorption. On the contrary, the imidazolium moiety takes part in electron acceptance from the filled d orbitals of Fe, resulting in retro-donation. DMIMHS is adsorbed onto the Fe and $FeCO_3$ surfaces *via* mixed adsorption, thus leading to the creation of protective layers on substrates.

In the light of theoretical evaluations, FMOs analysis, electrostatic potential analysis, reactivity indicators analysis and Fukui analysis were performed. The equilibrium adsorption configuration of CB6-based [3]rotaxane on the Fe(110) surface was successfully obtained through an MD simulation study.[97] From the side and top views, it can be observed that the IL is adsorbed onto the metal surface in a parallel fashion, as presented in Fig. 21(a). The IL can form a dense protective barrier onto the metal surface to prevent the penetration of corrosive particles, as observed in the density field distribution study, as presented in Fig. 21(b). Additionally, the parallel orientation of the IL after adsorption on the metal surface was confirmed by relative concentration distribution analysis, as presented in Fig. 21(c). The *z*-axis of the Fe(001) plane possesses a greater value of relative concentration. The relative

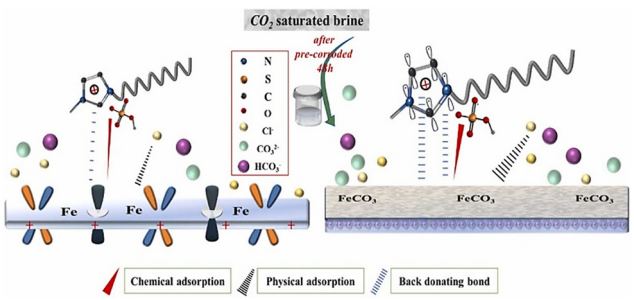

Fig. 20 Protective mechanism of DMIMHS towards the corrosion inhibition of Fe and $FeCO_3$ surface. [Reprinted with permission from ref. 119, ©2022 Elsevier.]

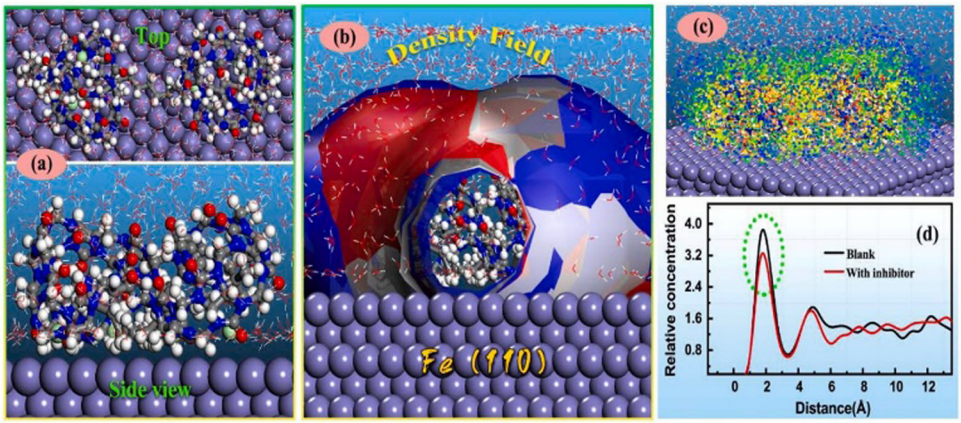

Fig. 21 (a) Optimized adsorption configuration of CB6-based [3]rotaxane on the Fe(110) surface, (b) density field distribution, (c) concentration distribution analysis, and (d) concentration distribution of water. [Reprinted with permission from ref. 97, ©2022 Elsevier.]

concentration of water molecules was found to increase in the absence of IL molecules, whereas it decreased in the presence of IL molecules. This signifies that the presence of IL molecules hinders the approach of water molecules towards the underlying metal body, as depicted in Fig. 21(d).

Again, the diffusion behaviour of a molecule can be reliably measured by its diffusion coefficient (D).[95] The diffusion coefficient indicates how fast a corrosive species can migrate in inhibitor films. Higher inhibition effectiveness results originate from lower D values, *i.e.*, a higher degree of corrosion prevention by the inhibitor film. The Einstein diffusion equation is typically used to obtain D from the mean square displacement (MSD). The MSD diagram through the inhibitor membranes displayed a subtle and minimal increase throughout the first simulation process. However, when the simulation period was prolonged, the MSD diagram showed a steady rise in the vacuum. The present D-values of H_2O computed in vacuum and membranes are 2.2×10^{-10} and 2.0×10^{-11} m^2 s^{-1}, respectively for thirty BKC cations and thirty chloride anions containing inhibitor film. Accordingly, the inhibitor membranes could efficiently restrict the migration of corrosive particles. For a better understanding, the free volume present within the inhibitor film was analyzed. The free volume within the inhibitor film indicates the available cavity for the migration of corrosive species. On the contrary, a small free volume indicates a better protective nature of the inhibitor. The equilibrium configuration and the free volume distribution with and without chloride ions are displayed in Fig. 22.

The fraction free volumes of the inhibitor film were 52% and 65% in the presence and absence of chloride ions, respectively. From these observations, it can be concluded that the presence of chloride ions has a huge impact on the protective nature of the inhibitors.[6,45]

7.4. Insight through MC simulation

Similar to the MD simulation, the MC simulation has become a popular computational simulation approach to comprehend

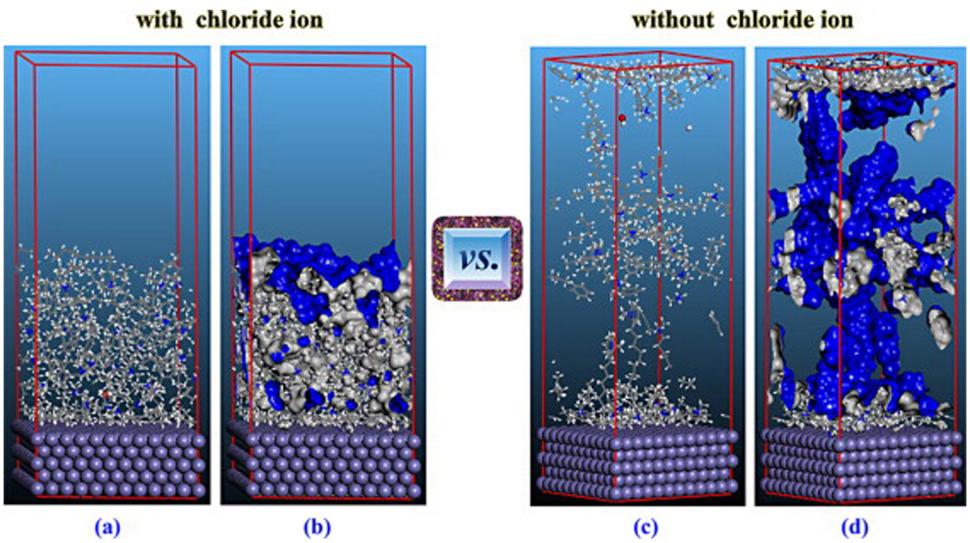

Fig. 22 (a) and (c) Equilibrium configuration and (b) and (d) free volume distribution of the inhibitor film of BKC cations with and without chloride ions.[Reprinted with permission from ref. 95, ©2015 Elsevier.]

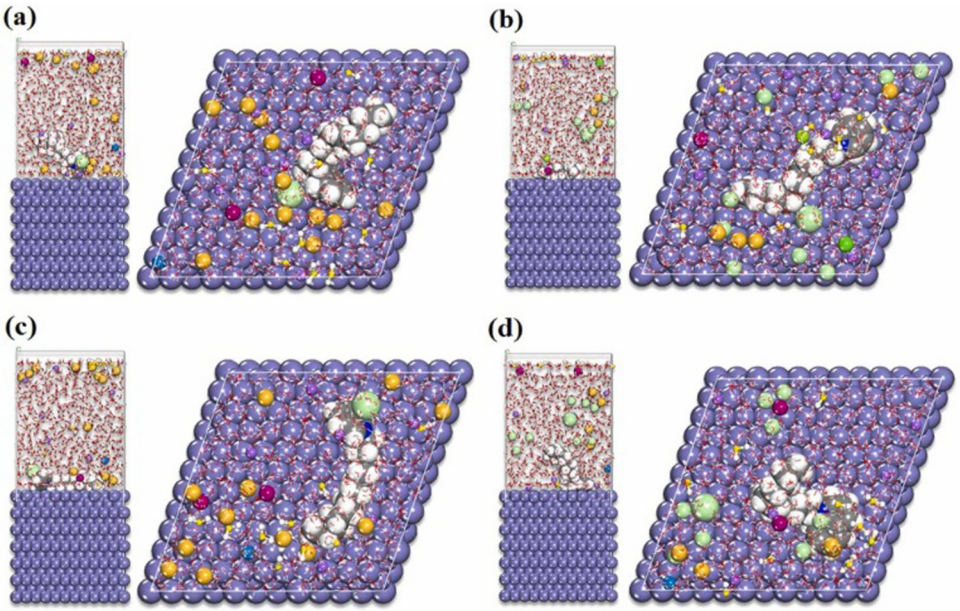

Fig. 23 Adsorption configurations obtained from (a) MC and (b) MD simulation for DDPC and (c) MC and (d) MD simulation for DDQC. [Reprinted with permission from ref. 105, ©2023 Elsevier.]

the as-desired observables. MC simulations are simpler than MD simulations because there is no need to consider forces.[135,154–156] The descriptors derived from MC simulation are as follows: total energy (E_T) represents the summation of the energies of the inhibitor and the metal surface; E_{ads} represents the energy released following the adsorption of the adsorbate molecules (herein, IL inhibitors); rigid energy (E_{rigid}) represents the energy released following the adsorption of one mole of energetically non-relaxed adsorbate; deformation energy (E_{def}) represents the energy released following the relaxation of one mole of adsorbate on the adsorbent surface; and the energy of the adsorbate following the removal of one adsorbate component denoted by dE_{ads}/dN_i.[157,158] By increasing the E_{ads} value, the interaction between the ILs and the metal is regarded to be stronger, that is better surface protection is achieved. Typically, the lowest energy adsorption sites are obtained using MC simulation techniques to determine the favoured adsorption sites on the metal surface. In several studies, MC simulation has been accepted as an efficient tool in determining the influence of the triggering effects on the adherence of the ILs on the metal surface.[42] Recently, an MC simulation study was performed to investigate the orientation of two PILs, namely, DDPC and DDQC, after adsorption on the metallic surface.[105] Fig. 23(a) and (c) depict the actual arrangement of the ILs. Herein, adsorption energies were obtained as −119.27 kcal mol^{-1} and −194.43 kcal mol^{-1} for DDPC and DDQC, respectively, that is DDQC served as a better surface protective agent and was further validated by theoretical analysis.

During the MC simulation, inhibitors were subjected to orient themselves in a horizontal fashion, in which pyridine rings orient themselves in a planar way in the ''decorative direction''. In this orientation, the heteroatoms, herein nitrogen, and electron-rich moieties come closer to the metal surface to make strong adsorption feasible.

7.5. Insight through QSAR analysis

QSAR analysis has now become an important tool to elucidate the relationship between the structural and physicochemical properties of ILs with corrosion inhibition efficiencies. To correlate the quantum chemical descriptors with the experimental findings, both linear and non-linear equations are used, as proposed by Lukovits.[159–162] These models include regression coefficients, various quantum chemical parameters and the experimental concentrations of the inhibitors. The linear and non-linear equations are expressed as mentioned in eqn (3) and (4), respectively:

$$IE_{theory} = AX_iC_i + B \quad (3)$$

$$IE_{theory} = \frac{(AX_i + B)C_i}{1 + (AX_i + B)C_i} \times 100 \quad (4)$$

where X_i and C_i are the quantum chemical index and experimental concentration of inhibitor I, respectively. A and B denote the regression coefficients determined through regression analysis. Several significant works regarding QSAR analysis have been found in the literature.

Seven linear equations and eight non-linear equations were developed by Murulana *et al.*[163] It has been observed that at least two quantum chemical parameters are absolutely necessary to achieve a strong agreement with the experimentally obtained results. Yesudass *et al.* investigated the correlation between the electronic parameters and subsequent corrosion inhibition efficiencies of five IMILs, namely, 1-ethyl-3-methylimidazolium ethylsulfate $[EMIM]^+$ $[EtSO_4]^-$, 1-ethyl-3-methylimidazolium acetate $[EMIM]^+$ $[Ac]^-$, 1-butyl-3-methylimidazolium thiocyanate $[BMIM]^+$ $[SCN]^-$, 1-butyl-3-methylimidazolium acetate $[BMIM]^+$ $[Ac]^-$ and 1-butyl-3-methylimidazolium dicyanamide $[BMIM]^+$ $[DCA]^-$ to suppress the mild steel

corrosion rate in HCl.[164] The QSAR analysis signifies that the IE of the ImILs is heavily influenced by the descriptors, including molecular weight, dipole moment and fraction of electron transferred from ImIL to the metal surface. The increased IE of $[EMIM]^+$ $[EtSO_4]^-$ compared to $[EMIM]^+$ $[Ac]^-$ is due to the presence of more electronegative heteroatoms, S than O. Besides, the presence of an extended alkyl chain within the $[BMIM]^+$ compared to $[EMIM]^+$ results in better IE in $[BMIM]^+$ series. In another study by Chen and co-workers, thirty-six ImILs with various anions, including halides, such as Cl^-, Br^-, and I^- along with $N(CN)_2^-$, BF_4^-, PF_6^- and varying alkyl chain lengths with 0, 1, 2, 3, 4, 5 and 6 number of carbons were studied to analyse the nature of adsorption on iron surface.[165] It was observed that the E_{ads} values of the ImILs were significantly influenced by the alkyl chain length of the cations, as demonstrated by applying the dispersion-corrected DFT (DFT-D3) method.

Additionally, DFT showed higher accuracy in predicting the adsorption process similar to MD simulation. It was observed that the E_{ads} value increased with the enhancement of the radius of the halides (*i.e.*, $Cl^- < Br^- < I^-$) for the first three ImILs. For the remaining three ImILs, BF_4^- and PF_6^- are adsorbed through fluorine atoms and $N(CN)_2^-$ is adsorbed through the N atom. To correlate the molecular descriptors with the DFT-calculated adsorption energies, the QSAR model was introduced. In this work, the training set and test set ratio was 80 : 20, and three machine learning algorithms (*e.g.*, multiple linear regression (MLR), random forest regression (RFR), and support vector regression (SVR)) were compared. Among the three algorithms, SVR achieved higher accuracy (coefficient of determination (R^2) $\sim$ 0.94) and lower error (Root Mean Square Error (RMSE) $\sim$ 10.2%). Accordingly, it was found that the QSAR model is suitable for predicting the adsorption energies of the ImILs. In a comprehensive theoretical analysis by Quadri *et al.*, traditional linear regression and non-linear multilayer perceptron neural network (MLPNN) were employed to establish the correlation between six selected descriptors and the experimental IE of the set of thirty ILs.[166] The linear model, with the sum of square error (SSE) 1156.53, demonstrated a moderate ability to describe the relationship between the selected sets of the DFT parameters obtained using the B3LYP functional and 6-31G+d,p basis set. However, a significantly improved model was achieved using standardized variables and a less biased MLPNN model. The non-linear model produced superior performance metrics, including a Mean Square Error (MSE) of 29.9242, RMSE of 5.4703, Median Absolute Deviation (MAD) of 4.9628 and Mean Absolute Percentage Error (MAPE) of 5.7809. Furthermore, the constructed models were used to theoretically evaluate the preventive performance of five new ILs to protect steel surfaces against HCl environments. In a recent study, the influence of alkyl chain lengths on the imidazolium cations and the size of the counter ions of six ImILs, namely, 1-ethyl-3-methylimidazolium chloride [EMIm Cl], 1-butyl-3-methylimidazolium chloride [BMIm Cl], 1-butyl-3-methylimidazolium hexafluorophosphate [BMIm PF6], 1-butyl-3-methylimidazolium tetrafluoroborate [BMIm BF4], 1-butyl-3-methylimidazolium bromide [BMIm Br], and 1-hexyl-3-methylimidazolium chloride [HMIm Cl], and their mixtures with an anionic surfactant, sodium dodecyl sulfate (SDS) on the IE of mild steel exposed to HCl was investigated through experimental, *ab initio* analysis and QSAR model.[151] The study revealed that an increase in the length of the alkyl chains or the size of the counter ions significantly increases the protective efficiency against corrosion. In this work, one linear and non-linear equations were developed to successfully correlate the quantum chemical parameters and experimentally obtain inhibition efficiencies. The high R^2 values (0.937 and 0.987), low SSE (0.003 and 0.005) and RMSE (0.0128 and 0.0059) for both the linear and non-linear equations indicate a strong relation between the dipole moment and the inhibition efficiencies. From the equations, it can be inferred that a high dipole moment contributes to a greater IE. A recent report unveiled the Group Contribution Method (GCM) accompanied by the QSAR model to carry out a more insightful investigation of seventy-four ILs as efficient corrosion inhibitors for the protection of carbon steel under a static HCl environment. Seventy-four ILs were categorized into twenty-nine functional groups of cations and seventeen functional groups of anions to acquire 760 data points. The model achieved good performance after the forth iteration by achieving the training sets (R^2 of 0.639 and average absolute average deviation (AARD) of 14.9%), a validation set (R^2 of 0.319 and AARD of 14.4%), and an overall data point assessment (R^2 of 0.324 and AARD of 14.3%).

8. Mechanism of adsorption on the iron surface

Similar to their traditional organic counterparts, ILs exert their effectiveness by obstructing both the anodic and cathodic sites on the metal surface. In simpler terms, these ILs impede or decelerate the rate of oxidation in the anode and reduction in the cathode (*i.e.*, redox reactions), introducing a deliberate slowdown to the chemical processes involved.[167–170]

According to Likhanova *et al.*, the redox reactions of a divalent metal in an acidic environment, *i.e.*, in presence of H_2SO_4 (SO_4^{2-} ion) and HCl (Cl^- ion), both with and without ILs, may be expressed as follows, as presented in eqn (5)–(8):[171]

(i) Anodic reactions in the absence of IL

$$M + nH_2O \leftrightarrow M(H_2O)_{n(ads)} \quad (5)$$

$$M(H_2O)_{n(ads)} + SO_4^{2-}/2Cl^- \leftrightarrow M[(H_2O)_nSO_4^{2-}/2Cl^-]_{ads} \quad (6)$$

$$M[(H_2O)_n\ SO_4^{2-}/2Cl^-]_{ads} \leftrightarrow M[(H_2O)_nSO_4/2Cl^-]_{ads} + 2e^- \quad (7)$$

$$M[(H_2O)_n\ SO_4/2Cl]_{ads} + 2e^- \leftrightarrow M^{2+} + OH^- + H^+ + SO_4^{2-}/2Cl^- \quad (8)$$

where M represents the metal element.

The SO_4^{2-} and Cl^- anions accelerate the anodic oxidation reactions. Alternatively, the introduction of IL hinders the anodic oxidation process due to the adsorption of the cations (IL^+) of these ILs. The quick oxidation of the metallic constituent results in electron gathering at the anodic site. Consequently, the cationic constituents of the ILs exhibit a preference for adsorption at the anodic site, thereby retarding the oxidation reaction. The underlying reaction mechanism is expressed using eqn (9):

(ii) Anodic reactions in the presence of IL

$$M[(H_2O)_nSO_4^{2-}/2Cl^-]_{ads} + IL^+ \leftrightarrow M[(H_2O)_nSO_4/2Cl\ IL]_{ads}^- \quad (9)$$

The adsorption of cations at the anode is accelerated by counter ions, such as sulphate and chloride ions.

(iii) Cathodic reactions in the absence of IL

When corrosion inhibiting substances are not present in aqueous electrolytes, cathodic reactions occur, as shown in eqn (10)–(12):

$$M + H_3O^+ \leftrightarrow M(H_3O)_{ads}^+ \quad (10)$$

$$M(H_3O)_{ads}^+ \leftrightarrow M(H_3O)_{ads} + e^- \quad (11)$$

$$M(H_3O)_{ads} + e^- + H^+ \leftrightarrow M + H_2O + H_2 \quad (12)$$

(iv) Cathodic reactions in the presence of IL, as denoted in eqn (13) and (14):

$$M + IL^+ \leftrightarrow M(IL)_{ads}^+ \quad (13)$$

$$M(IL)_{ads}^+ + e^- \leftrightarrow M(IL)_{ads} \quad (14)$$

Typically, the adsorption of ILs occurs due to electrostatic forces between the charged metal surface and inhibitors. However, after adsorption, cationic species acquire electrons and undergo a transformation into neutral forms. Uncharged entities possessing available unshared paired electrons become adsorbed by transferring their non-bonding and/or π-electrons into the d-orbitals of the metal *via* chemisorption. Because metals are inherently electron-rich, electron transfer leads to inter-electronic repulsion, prompting the metal to transfer its electrons back to the anti-bonding molecular orbitals of the inhibitor through a process known as retro-donation. Mutual electron donation and retro-donation enhance chemical bonding synergistically. The presence of IL significantly retards the corrosion rate, as illustrated in Fig. 24.[172–174] It has been observed that in the presence of a corrosive medium (herein, HCl), Cl- ions are first adsorbed onto the iron surface, which further produces Fe^{2+} and Fe^{3+} ions through the oxidation process on the anodic side. The major corrosive products formed are $Fe(OH)_3$, $Fe(OH)_2$, α-FeOOH, and γ-FeOOH. The α-FeOOH and γ-FeOOH are called 'green rust'. On the cathodic side, H_2O and H_2 are produced as reduced products of H_3O^+. Accordingly, the metal surface deteriorates. When ILs are added to the corrosive medium, they form a dense film on the metal surface. The ILs interact with the metal surface *via* physisorption (*i.e.*, electrostatic interaction), chemisorption (*i.e.*, electron transfer from filled non-bonded orbitals of heteroatoms, such as N and O of any functional group, such as –OH, $–NH_2$, and –SH, or electron transfer from π-orbitals to the vacant d-orbitals of iron), and retro-donation from filled d-orbital of Fe to the vacant π-orbitals of inhibitors. Consequently, the approach of corrosive species, such as Cl^-, H_2O and H_3O^+, is hindered. The adsorption of ILs as corrosion inhibitors on iron surfaces occurs through complex interactions involving both electrostatic and chemisorption mechanisms. The initial stage typically involves the adsorption of charged IL components, such as anions or cations, onto the metal surface driven by electrostatic forces. For example, anions, such as I^-, with a high electron density can readily donate electrons to iron atoms, facilitating the subsequent adsorption of the imidazolium cation. This initial adsorption of I^- ions creates a negatively charged layer on the metal surface, attracting counter-ions from the IL bulk solution.[174,175]

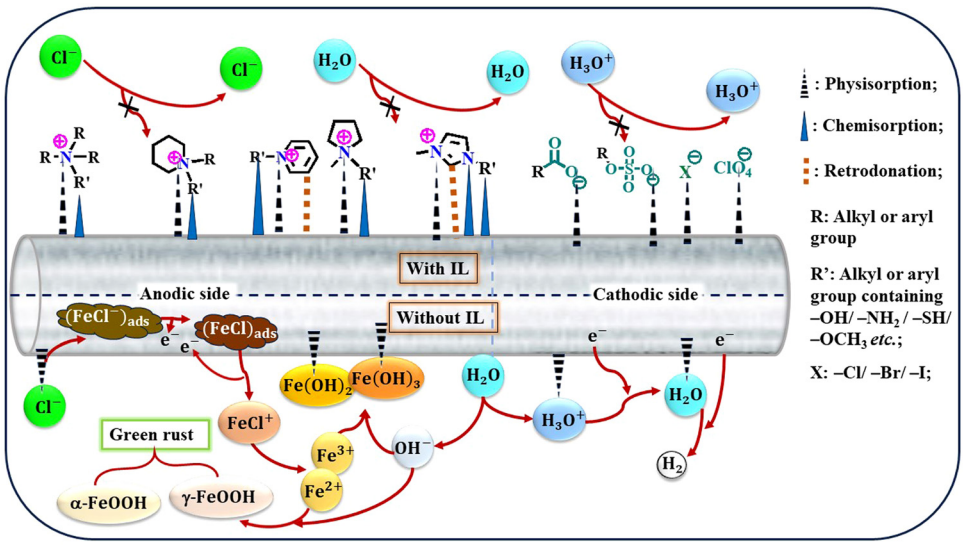

Fig. 24 Mechanism of corrosion within HCl environment and mechanism of corrosion retardation process in the presence of IL.

Furthermore, chemisorption plays a crucial role in anchoring ILs to the metal surface. Specific functional groups present in the ILs, such as the –N=C–N moiety in ImILs, act as active adsorption centres. These groups can form strong chemical bonds with the iron atoms through donor–acceptor interactions, involving the lone pairs of electrons on the N-atoms and the unoccupied orbitals on the Fe. The extent of chemisorption is influenced by factors such as the type of functional groups, the structure of the ILs, and the surface properties of the iron. This combined action of electrostatic and chemisorption mechanisms leads to the development of a stable shield on the iron surface. This film effectively blocks the active sites of corrosion, which hinders the migration of corrosive species to the metal surface, thereby preventing the occurrence of the redox process involved in corrosion. The adsorption phenomena are influenced by various factors such as the concentration of the ILs, the temperature, and the presence of other species in the electrolyte. Understanding the specific adsorption mechanism of each IL-iron system is crucial for optimizing the design and application of these promising corrosion inhibitors.

9. Conclusion and future perspectives

In conclusion, the quest for green and sustainable corrosion prevention technologies has led to a significant focus on the application of ILs as next-generation corrosion inhibitors. Over the past decade, the escalating awareness of ecological considerations and the imposition of stringent environmental regulations have underscored the paramount importance of advancing corrosion mitigation methods. In response to these requirements, ILs have emerged as promising contenders, endowed with unique properties, such as low volatility, non-flammability, and high thermal and chemical stability. Their exceptional ability to get adsorbed onto various metallic surfaces adds versatility to their protective function. This comprehensive review has thoroughly explored the diverse applications of N^+-containing ILs as efficient corrosion inhibitors for the protection of steel surfaces in diverse corrosive mediums. This exploration extends across various electrolytic environments, providing insights into the adaptability and efficacy of ILs in different corrosion scenarios.

Moreover, the review delves into the intricate mechanisms and adsorption behaviours of ILs on metallic surfaces. A concerted effort is made to employ state-of-the-art experimental and computational approaches to ensure a nuanced and comprehensive understanding of the corrosion inhibition potential of ILs. This amalgamation of methodologies advances our knowledge and positions ILs as transformative agents in the field of sustainable corrosion prevention.

As the global community increasingly recognizes the importance of eco-friendly practices and stringent adherence to environmental standards, the role of ILs in corrosion science becomes more pronounced. Their promise as agents of change in sustainable materials protection resonates as a beacon for future endeavours in corrosion research and underscores the ongoing evolution towards greener technologies in corrosion prevention.

Future avenues for exploration

Next-Gen ILs. Research efforts should continue to focus on the development of ILs with enhanced corrosion inhibition performance for specific metals and alloys, particularly under extreme environmental conditions.

Synergistic effects. Exploring synergistic effects between ILs and other corrosion inhibitors holds significant promise for achieving superior protection and expanding the application scope of ILs.

Predictive power. Advanced computational models should be developed to accurately predict the corrosion inhibition efficacy of ILs, facilitating the design and selection of optimal ILs for specific needs.

Long-term sustainability. Investigating the long-term stability and potential environmental impact of ILs in real-world applications is crucial for ensuring their sustainable and responsible implementation.

In a nutshell, this review has portrayed a vivid picture of the tremendous potential of ILs as game changers in the field of corrosion inhibition. By leveraging their unique properties, tunability, and environmental compatibility, ILs are poised to revolutionize this field, ushering in a new era of sustainable and effective corrosion protection. By pursuing further research focused on addressing their current limitations and exploring their full potential, we can pave the way for the widespread adoption of these remarkable materials, thereby contributing to a more sustainable future for our planet and its resources.

Author contributions

Sanjukta Zamindar: conceptualization, methodology, software, visualization, writing – original draft preparation. Sukdeb Mandal: visualization, writing – reviewing and editing. Manilal Murmu: investigation, validation, writing – reviewing and editing. Priyabrata Banerjee: supervision, validation, writing – reviewing and editing.

Conflicts of interest

There are no conflicts to declare.

Acknowledgements

The PB is very thankful to the Science and Engineering Research Board, Department of Science and Technology, Government of India (project no. GAP-240712, reference no. 01DU20003A). SZ acknowledges the Department of Science and Technology (DST), Government of India, for her fellowship (IF200407). SM acknowledges the University Grants Commission (UGC), Government of India, for his fellowship [212/CSIR-UGC NET DEC.2017].

References

1 A. G. Nurioglu, A. C. C. Esteves and G. de With, *J. Mater. Chem. B*, 2015, **3**, 6547–6570.
2 U. Z. Husna, K. A. Elraies, J. A. B. M. Shuhili and A. A. Elryes, *J. Pet. Explor. Prod. Technol.*, 2022, **12**, 1075–1094.
3 C. Verma, D. K. Verma, E. E. Ebenso and M. A. Quraishi, *Heteroat. Chem.*, 2018, **29**, e21437.
4 M. J. Nine, M. A. Cole, D. N. H. Tran and D. Losic, *J. Mater. Chem. A*, 2015, **3**, 12580–12602.
5 P. Banerjee, M. Murmu, S. Zamindar and N. C. Murmu, *Carbon Allotropes*, De Gruyter, 2022, pp. 175–200.
6 S. Gurjar, S. K. Sharma, A. Sharma and S. Ratnani, *Appl. Surf. Sci. Adv.*, 2021, **6**, 100170.
7 A. R. Prasad, A. Kunyankandy and A. Joseph, *Corrosion Inhibitors in the Oil and Gas Industry*, Wiley, 2020, pp. 135–150.
8 B. D. B. Tiu and R. C. Advincula, *React. Funct. Polym.*, 2015, **95**, 25–45.
9 N. Tiwari, R. K. Mitra and M. Yadav, *Surf. Interfaces*, 2021, **22**, 100770.
10 M. Murmu, S. K. Saha, N. C. Murmu and P. Banerjee, *J. Mol. Liq.*, 2019, **278**, 521–535.
11 B. Kulyk, M. A. Freitas, N. F. Santos, F. Mohseni, A. F. Carvalho, K. Yasakau, A. J. S. Fernandes, A. Bernardes, B. Figueiredo, R. Silva, J. Tedim and F. M. Costa, *Crit. Rev. Solid State Mater. Sci.*, 2021, 1–48.
12 R. Ding, W. Li, X. Wang, T. Gui, B. Li, P. Han, H. Tian, A. Liu, X. Wang, X. Liu, X. Gao, W. Wang and L. Song, *J. Alloys Compd.*, 2018, **764**, 1039–1055.
13 A. Dehghani, G. Bahlakeh and B. Ramezanzadeh, *Chem. Eng. J.*, 2020, **400**, 125860.
14 A. Singh, K. R. Ansari, P. Bedi, T. Pramanik, I. H. Ali, Y. Lin, P. Banerjee and S. Zamindar, *J. Phys. Chem. Solids*, 2023, **172**, 111064.
15 M. Mobin Huda, S. Zamindar and P. Banerjee, *J. Mol. Liq.*, 2023, **385**, 122403.
16 J. Haque, V. Srivastava, M. A. Quraishi, D. Singh Chauhan, H. Lgaz and I.-M. Chung, *Corros. Sci.*, 2020, **172**, 108665.
17 S. K. Saha, M. Murmu, N. C. Murmu and P. Banerjee, *J. Mol. Struct.*, 2021, **1245**, 131098.
18 M. O. Valappil, F. Forouzandeh, X. Li, S. Luong, M. Atwa and V. I. Birss, *Electrochim. Acta*, 2022, **422**, 140444.
19 M. Ozhukil Valappil, F. Forouzandeh, M. Atwa, S. Luong and V. I. Birss, *ECS Meet. Abstr.*, 2021, **MA2021–02**, 541.
20 F. Forouzandeh, X. Li, D. W. Banham, F. Feng, S. Ye and V. Birss, *J. Electrochem. Soc.*, 2018, **165**, F3230–F3240.
21 R. P. Wong, J. E. Wong and V. I. Birss, *Can. J. Chem.*, 2004, **82**, 1536–1544.
22 J. Wang, L. An, J. Wang, J. Gu, J. Sun and X. Wang, *Adv. Colloid Interface Sci.*, 2023, **321**, 103031.
23 J. Saranya, M. Sowmiya, P. Sounthari, K. Parameswari, S. Chitra and K. Senthilkumar, *J. Mol. Liq.*, 2016, **216**, 42–52.
24 N. N. Hau and D. Q. Huong, *J. Mol. Struct.*, 2023, **1277**, 134884.
25 S. Vikneshvaran and S. Velmathi, *ChemistrySelect*, 2019, **4**, 387–392.
26 N. K. Gupta, C. Verma, R. Salghi, H. Lgaz, A. K. Mukherjee and M. A. Quraishi, *New J. Chem.*, 2017, **41**, 13114–13129.
27 H. Assad and A. Kumar, *J. Mol. Liq.*, 2021, **344**, 117755.
28 C. Verma, L. O. Olasunkanmi, E. E. Ebenso and M. A. Quraishi, *J. Mol. Liq.*, 2018, **251**, 100–118.
29 R. Aslam, G. Serdaroglu, S. Zehra, D. Kumar Verma, J. Aslam, L. Guo, C. Verma, E. E. Ebenso and M. A. Quraishi, *J. Mol. Liq.*, 2022, **348**, 118373.
30 D. S. Chauhan, C. Verma and M. A. Quraishi, *J. Mol. Struct.*, 2021, **1227**, 129374.
31 X. Ren, S. Xu, X. Gu, B. Tan, J. Hao, L. Feng, W. Ren, F. Gao, S. Zhang, Y. Xiao and L. Huang, *J. Colloid Interface Sci.*, 2021, **585**, 614–626.
32 D. Sukul, A. Pal, S. K. Saha, S. Satpati, U. Adhikari and P. Banerjee, *Phys. Chem. Chem. Phys.*, 2018, **20**, 6562–6574.
33 R. Aslam, M. Mobin Huda, M. Shoeb, M. Murmu and P. Banerjee, *J. Ind. Eng. Chem.*, 2021, **100**, 333–350.
34 M. Mobin Huda, M. Shoeb, R. Aslam and P. Banerjee, *J. Mol. Struct.*, 2022, **1262**, 133027.
35 A. Singh, K. R. Ansari, I. H. Ali, Y. Lin, M. Murmu and P. Banerjee, *J. Mol. Liq.*, 2023, **376**, 121408.
36 C. Verma, E. E. Ebenso and M. A. Quraishi, *J. Mol. Liq.*, 2017, **233**, 403–414.
37 K. Goossens, K. Lava, C. W. Bielawski and K. Binnemans, *Chem. Rev.*, 2016, **116**, 4643–4807.
38 S. N. Pedro, C. S. R. Freire, A. J. D. Silvestre and M. G. Freire, *Int. J. Mol. Sci.*, 2020, **21**, 8298.
39 C. Verma, L. O. Olasunkanmi, I. Bahadur, H. Lgaz, M. A. Quraishi, J. Haque, E.-S. M. Sherif and E. E. Ebenso, *J. Mol. Liq.*, 2019, **273**, 1–15.
40 T. Gu, Z. Chen, X. Jiang, L. Zhou, Y. Liao, M. Duan, H. Wang and Q. Pu, *Corros. Sci.*, 2015, **90**, 118–132.
41 C. Verma, E. E. Ebenso, M. A. Quraishi and C. M. Hussain, *Mater. Adv.*, 2021, **2**, 3806–3850.
42 R. Aslam, M. Mobin Huda, M. Murmu, P. Banerjee and J. Aslam, *J. Mol. Liq.*, 2021, **334**, 116469.
43 A. Singh, K. R. Ansari, M. A. Quraishi and P. Banerjee, *J. Mol. Liq.*, 2021, **323**, 114608.
44 E. Berdimurodov, A. Kholikov, K. Akbarov, L. Guo, S. Kaya, K. P. Katin, D. Kumar Verma, M. Rbaa, O. Dagdag and R. Haldhar, *J. Electroanal. Chem.*, 2021, **901**, 115794.
45 L. Souza, E. Pereira, L. Matlakhova, V. A. F. Nicolin, S. N. Monteiro and A. R. G. de Azevedo, *J. Mater. Res. Technol.*, 2023, **22**, 2186–2205.
46 Y. L. Kobzar and K. Fatyeyeva, *Chem. Eng. J.*, 2021, **425**, 131480.
47 S. K. Singh and A. W. Savoy, *J. Mol. Liq.*, 2020, **297**, 112038.
48 K. J. Kulacki and G. A. Lamberti, *Green Chem.*, 2008, **10**, 104–110.
49 M. Kumar, N. Trivedi, C. R. K. Reddy and B. Jha, *Chem. Res. Toxicol.*, 2011, **24**, 1882–1890.
50 L. Ma, Q. Lin, Y. Song, B. Zhao and M. Fan, *Open Life Sci.*, 2020, **15**, 466–475.
51 S. Sugden and H. Wilkins, *J. Chem. Soc.*, 1929, 1291–1298.
52 Z. Lei, B. Chen, Y.-M. Koo and D. R. MacFarlane, *Chem. Rev.*, 2017, **117**, 6633–6635.

53 Q. Zhang and J. M. Shreeve, *Chem. Rev.*, 2014, **114**, 10527–10574.
54 C. Reichardt, *J. Org. Chem.*, 2022, **87**, 1616–1629.
55 R. Hayes, G. G. Warr and R. Atkin, *Chem. Rev.*, 2015, **115**, 6357–6426.
56 F. Javed, F. Ullah, M. R. Zakaria and H. M. Akil, *J. Mol. Liq.*, 2018, **271**, 403–420.
57 A. R. Hajipour and F. Rafiee, *Org. Prep. Proced. Int.*, 2015, **47**, 249–308.
58 A. P. M. Tavares, O. Rodríguez and E. A. Macedo, *Ionic Liquids—New Aspects for the Futureed*, ed. J.-I. Kadokawa, InTech, Rijeka, Croatia, 2013, ch. 20, p. 537.
59 J. S. Wilkes and M. J. Zaworotko, *J. Chem. Soc., Chem. Commun.*, 1992, 965.
60 M. D. Morton and C. K. Hamer, *Sep. Purif. Technol.*, 2018, **196**, 3–9.
61 S. Zafari, A. A. Sarabi and B. Movassagh, *Corros. Eng. Sci. Technol.*, 2020, **55**, 589–601.
62 S. Cao, D. Liu, H. Ding, J. Wang, H. Lu and J. Gui, *Corros. Sci.*, 2019, **153**, 301–313.
63 J. S. Sandhu, *Green Chem. Lett. Rev.*, 2011, **4**, 289–310.
64 T. L. Greaves and C. J. Drummond, *Chem. Rev.*, 2008, **108**, 206–237.
65 C. A. Angell, N. Byrne and J.-P. Belieres, *Acc. Chem. Res.*, 2007, **40**, 1228–1236.
66 A. Kuchenbuch and R. Giernoth, *ChemistryOpen*, 2015, **4**, 677–681.
67 P. Sun and D. W. Armstrong, *Anal. Chim. Acta*, 2010, **661**, 1–16.
68 S. Jeong, S. Li, G. B. Appetecchi and S. Passerini, *Energy Storage Mater.*, 2019, **18**, 1–9.
69 M. Deetlefs, K. R. Seddon and M. Shara, *Phys. Chem. Chem. Phys.*, 2006, **8**, 642–649.
70 S. Dewilde, W. Dehaen and K. Binnemans, *Green Chem.*, 2016, **18**, 1639–1652.
71 T. L. Greaves and C. J. Drummond, *Chem. Soc. Rev.*, 2008, **37**, 1709.
72 N. V. Plechkova and K. R. Seddon, *Chem. Soc. Rev.*, 2008, **37**, 123–150.
73 J. Flieger and M. Flieger, *Int. J. Mol. Sci.*, 2020, **21**, 6267.
74 H.-B. Wu, B. Zhang, S.-H. Liu and C.-C. Chen, *J. Loss Prev. Process Ind.*, 2020, **66**, 104196.
75 T. Nakashima and N. Kimizuka, *Polym. J.*, 2012, **44**, 665–671.
76 B. Nanda, M. S. Sailu, P. M. Priyaranjan, R. K. P. Ranjan and B. M. Nanda, *Mater. Today Proc.*, 2021, **47**(5), 1234–1240.
77 Himani, A. Pratap Singh Raman, M. Babu Singh, P. Jain, P. Chaudhary, I. Bahadur, K. Lal, V. Kumar and P. Singh, *J. Mol. Liq.*, 2022, **364**, 119989.
78 K. Sood, Y. Saini and K. K. Thakur, *Mater. Today Proc.*, 2023, **81**, 739–744.
79 P. Izák, F. D. Bobbink, M. Hulla, M. Klepic, K. Friess, Š. Hovorka and P. J. Dyson, *ChemPlusChem*, 2018, **83**, 7–18.
80 M.-D. Bermúdez, A.-E. Jiménez, J. Sanes and F.-J. Carrión, *Molecules*, 2009, **14**, 2888–2908.
81 L. Chen, M. Sharifzadeh, N. Mac Dowell, T. Welton, N. Shah and J. P. Hallett, *Green Chem.*, 2014, **16**, 3098–3106.
82 Z. Zhou, H. Matsumoto and K. Tatsumi, *Chem. – Eur. J.*, 2005, **11**, 752–766.
83 M. Yoshizawa, W. Xu and C. A. Angell, *J. Am. Chem. Soc.*, 2003, **125**, 15411–15419.
84 F. Philippi and T. Welton, *Phys. Chem. Chem. Phys.*, 2021, **23**, 6993–7021.
85 J.-M. Lee, *Chem. Eng. J.*, 2011, **172**, 1066–1071.
86 H. Asfour, G. Y. Elewady, E. G. Zaki and A. E.-A. S. Fouda, *ACS Omega*, 2023, **8**, 41077–41099.
87 S. Herrmann, M. Kostrzewa, A. Wierschem and C. Streb, *Angew. Chem., Int. Ed.*, 2014, **53**, 13596–13599.
88 M. Mobin, R. Aslam, R. Salim and S. Kaya, *J. Colloid Interface Sci.*, 2022, **620**, 293–312.
89 S. Gao, Y. Huang, Y. Xiong, X. Guo, J. Zhang and L. Wang, *J. Mol. Liq.*, 2023, **386**, 122467.
90 P. Arellanes-Lozada, O. Olivares-Xometl, N. V. Likhanova, I. V. Lijanova, J. R. Vargas-García and R. E. Hernández-Ramírez, *J. Mol. Liq.*, 2018, **265**, 151–163.
91 E. Udabe, M. Forsyth, A. Somers and D. Mecerreyes, *Mater. Adv.*, 2020, **1**, 584–589.
92 H. M. Abd El-Lateef, A. H. Tantawy and A. A. Abdelhamid, *J. Surfactants Deterg.*, 2017, **20**, 735–753.
93 O. Olivares-Xometl, E. Álvarez-Álvarez, N. V. Likhanova, I. V. Lijanova, R. E. Hernández-Ramírez, P. Arellanes-Lozada and J. L. Varela-Caselis, *J. Adhes. Sci. Technol.*, 2018, **32**, 1092–1113.
94 P. Arellanes-Lozada, O. Olivares-Xometl, N. V. Likhanova, E. M. Arce-Estrada, I. V. Lijanova, L. Lartundo-Rojas and M. de Consuelo Mendoza-Herrera, *Int. J. Electrochem. Sci.*, 2016, **11**, 7785–7800.
95 L. Guo, S. Zhu and S. Zhang, *J. Ind. Eng. Chem.*, 2015, **24**, 174–180.
96 A. Dhawan, B. A. Laurent, J. Moloney and C. M. Silvernail, Molecules having one hydrophobic group and two identical hydrophilic ionic groups and compositions thereof, *Australia Pat.*, AU2021204283B2, September 22, 2022.
97 E. Berdimurodov, A. Kholikov, K. Akbarov, L. Guo, S. Kaya, K. P. Katin, D. K. Verma, M. Rbaa and O. Dagdag, *Colloids Surf., A*, 2022, **633**, 127837.
98 S. Zehra, M. Mobin, R. Aslam, H. Lgaz and I.-M. Chung, *J. Mol. Struct.*, 2021, **1240**, 130505.
99 E. Li, Y. Li, S. Liu and P. Yao, *Colloids Surf., A*, 2023, **657**, 130541.
100 A. Singh, K. R. Ansari, P. Banerjee, M. Murmu, M. A. Quraishi and Y. Lin, *Colloids Surf., A*, 2021, **623**, 126708.
101 B. Anandkumar, R. P. George and J. Philip, *Anal. Chim. Acta*, 2020, **1126**, 38–51.
102 S. M. Ali, K. M. Emran and M. Messali, *Prog. Org. Coat.*, 2019, **130**, 226–234.
103 F. El-Hajjaji, E. Ech-chihbi, N. Rezki, F. Benhiba, M. Taleb, D. S. Chauhan and M. A. Quraishi, *J. Mol. Liq.*, 2020, **314**, 113737.

104 F. E. L. Hajjaji, R. Salim, M. Taleb, F. Benhiba, N. Rezki, D. S. Chauhan and M. A. Quraishi, *Surf. Interfaces*, 2021, **22**, 100881.
105 D. Iravani, N. Esmaeili, A. Berisha, E. Akbarinezhad and M. H. Aliabadi, *Colloids Surf., A*, 2023, **656**, 130544.
106 M. Messali, S. M. Almutairi, A. Ait Mansour, R. Salghi and H. Lgaz, *J. Mater. Res. Technol.*, 2023, **27**, 8292–8307.
107 S. Ben Aoun, *RSC Adv.*, 2017, **7**, 36688–36696.
108 E. K. Ardakani, E. Kowsari, A. Ehsani and S. Ramakrishna, *Microchem. J.*, 2021, **165**, 106049.
109 A. M. El-Shamy, K. Zakaria, M. A. Abbas and S. Zein El Abedin, *J. Mol. Liq.*, 2015, **211**, 363–369.
110 M. Zunita and Y. J. Kevin, *Results Eng.*, 2022, **15**, 100562.
111 A. H. E. Moustafa, H. H. Abdel-Rahman, M. Hagar, M. R. Aouad, N. Rezki and S. A. A. Bishr, *Sci. Rep.*, 2023, **13**, 19197.
112 O. Al-Rashed and A. Abdel Nazeer, *Materials*, 2022, **15**, 2326.
113 M. D. Green and T. E. Long, *Polym. Rev.*, 2009, **49**, 291–314.
114 S. Velusamy, S. Sakthivel, L. Neelakantan and J. S. Sangwai, *J. Earth Sci.*, 2017, **28**, 949–961.
115 M. T. Zaky, M. I. Nessim and M. A. Deyab, *J. Mol. Liq.*, 2019, **290**, 111230.
116 C. Liu, P. Du, F. Nan, H. Zhao and L. Wang, *Surf. Topogr.: Metrol. Prop.*, 2018, **6**, 024004.
117 E. Kowsari, M. Payami, R. Amini, B. Ramezanzadeh and M. Javanbakht, *Appl. Surf. Sci.*, 2014, **289**, 478–486.
118 I. Lozano, E. Mazario, C. O. Olivares-Xometl, N. V. Likhanova and P. Herrasti, *Mater. Chem. Phys.*, 2014, **147**, 191–197.
119 Y. Guo, J. Xue, J. Zhang, Q. Chen, L. Fan, C. Tang, K. Ren, A. Fu and Q. Bi, *Colloids Surf., A*, 2022, **651**, 129135.
120 S. Cao, D. Liu, H. Ding, H. Lu and J. Gui, *J. Colloid Interface Sci.*, 2020, **579**, 315–329.
121 E. E. El-Katori, M. I. Nessim, M. A. Deyab and K. Shalabi, *J. Mol. Liq.*, 2021, **337**, 116467.
122 L. Feng, S. Zhang, Y. Qiang, S. Xu, B. Tan and S. Chen, *Mater. Chem. Phys.*, 2018, **215**, 229–241.
123 R. Haldhar, C. Jayprakash Raorane, V. K. Mishra, T. Periyasamy, A. Berisha and S.-C. Kim, *J. Mol. Liq.*, 2023, **372**, 121168.
124 F. El Hajjaji, E. Ech-chihbi, R. Salim, A. Titi, M. Messali, B. El Ibrahimi, S. Kaya and M. Taleb, *Mater. Sci. Eng. B*, 2023, **289**, 116232.
125 X. Zeng, X. Zheng, L. Guo, Q. Xu, H. Huang and B. Tan, *J. Mol. Liq.*, 2021, **324**, 115063.
126 Bhaskaran, P. D. Pancharatna, S. Lata and G. Singh, *J. Mol. Liq.*, 2019, **278**, 467–476.
127 S. Cao, D. Liu, H. Ding, J. Wang, H. Lu and J. Gui, *J. Mol. Liq.*, 2019, **275**, 729–740.
128 M. Talebian, K. Raeissi, M. Atapour, B. M. Fernández-Pérez, Z. Salarvand, S. Meghdadi, M. Amirnasr and R. M. Souto, *Appl. Surf. Sci.*, 2018, **447**, 852–865.
129 L. Feng, S. Zhang, Y. Lu, B. Tan, S. Chen and L. Guo, *Appl. Surf. Sci.*, 2019, **483**, 901–911.
130 O. A. Al-Rashed and A. A. Nazeer, *J. Mol. Liq.*, 2019, **288**, 111015.
131 E. E. Ebenso, C. Verma, L. O. Olasunkanmi, E. D. Akpan, D. K. Verma, H. Lgaz, L. Guo, S. Kaya and M. A. Quraishi, *Phys. Chem. Chem. Phys.*, 2021, **23**, 19987–20027.
132 A. A. Bahraq, I. B. Obot, M. A. Al-Osta and M. Ibrahim, *Constr. Build. Mater.*, 2024, **412**, 134808.
133 C. Verma, M. A. Quraishi and K. Y. Rhee, *Chem. Eng. J.*, 2022, **430**, 132645.
134 S. Donkor, Z. Song, L. Jiang and H. Chu, *J. Mol. Liq.*, 2022, **359**, 119260.
135 C. Verma, H. Lgaz, D. K. Verma, E. E. Ebenso, I. Bahadur and M. A. Quraishi, *J. Mol. Liq.*, 2018, **260**, 99–120.
136 S. K. Saha, P. Ghosh, A. Hens, N. C. Murmu and P. Banerjee, *Phys. E*, 2015, **66**, 332–341.
137 S. Sengupta, M. Murmu, S. Mandal, H. Hirani and P. Banerjee, *Colloids Surf., A*, 2021, **617**, 126314.
138 S. Mandal, S. Zamindar, S. Sarkar, M. Murmu, L. Guo, S. Kaya, H. Hirani and P. Banerjee, *J. Adhes. Sci. Technol.*, 2022, 1–17.
139 S. Mandal, S. Bej and P. Banerjee, *J. Mol. Liq.*, 2023, **381**, 121789.
140 X. Zheng, S. Zhang, M. Gong and W. Li, *Ind. Eng. Chem. Res.*, 2014, **53**, 16349–16358.
141 L. Guo, C. Qi, X. Zheng, R. Zhang, X. Shen and S. Kaya, *RSC Adv.*, 2017, **7**, 29042–29050.
142 S. K. Saha, A. Dutta, P. Ghosh, D. Sukul and P. Banerjee, *Phys. Chem. Chem. Phys.*, 2016, **18**, 17898–17911.
143 J. Li, *Handbook of Materials Modeling*, Ohio State University, 2005, pp. 565–588.
144 S. K. Saha, A. Dutta, P. Ghosh, D. Sukul and P. Banerjee, *Phys. Chem. Chem. Phys.*, 2015, **17**, 5679–5690.
145 S. Kaya, B. Tüzün, C. Kaya and I. B. Obot, *J. Taiwan Inst. Chem. Eng.*, 2016, **58**, 528–535.
146 N. I. N. Haris, S. Sobri, Y. A. Yusof and N. K. Kassim, *Metals*, 2020, **11**, 46.
147 S. Kaya, P. Banerjee, S. K. Saha, B. Tüzün and C. Kaya, *RSC Adv.*, 2016, **6**, 74550–74559.
148 M. Murmu, S. Sengupta, R. Pal, S. Mandal, N. C. Murmu and P. Banerjee, *RSC Adv.*, 2020, **10**, 33401–33416.
149 C. Verma, L. O. Olasunkanmi, I. B. Obot, E. E. Ebenso and M. A. Quraishi, *RSC Adv.*, 2016, **6**, 53933–53948.
150 R. Hsissou, F. Benhiba, O. Dagdag, M. El Bouchti, K. Nouneh, M. Assouag, S. Briche, A. Zarrouk and A. Elharfi, *J. Colloid Interface Sci.*, 2020, **574**, 43–60.
151 A. Yousefi, S. Javadian, N. Dalir, J. Kakemam and J. Akbari, *RSC Adv.*, 2015, **5**, 11697–11713.
152 R. Hsissou, F. Benhiba, M. El Aboubi, S. Abbout, Z. Benzekri, Z. Safi, M. Rafik, H. Bahaj, M. Kaba, M. Galai, N. Wazzan, S. Briche, S. Boukhris, A. Zarrouk, M. EbnTouhami and M. Rafik, *Chem. Phys. Lett.*, 2022, **806**, 139995.
153 A. Singh, K. R. Ansari, Y. Lin, M. A. Quraishi, H. Lgaz and I.-M. Chung, *J. Taiwan Inst. Chem. Eng.*, 2019, **95**, 341–356.
154 L. H. Madkour, S. Kaya and I. B. Obot, *J. Mol. Liq.*, 2018, **260**, 351–374.
155 K. F. Khaled and A. El-Maghraby, *Arab. J. Chem.*, 2014, **7**, 319–326.

156 A. Kasprzhitskii and G. Lazorenko, *J. Mol. Liq.*, 2021, **331**, 115782.
157 K. Cherrak, M. E. Belghiti, A. Berrissoul, M. El Massaoudi, M. El Faydy, M. Taleb, S. Radi, A. Zarrouk and A. Dafali, *Surf. Interfaces*, 2020, **20**, 100578.
158 H. El Aadad, M. Galai, M. Ouakki, A. Elgendy, M. E. Touhami and A. Chahine, *Surf. Interfaces*, 2021, **24**, 101084.
159 I. Lukovits, I. Bakó, A. Shaban and E. Kálmán, *Electrochim. Acta*, 1998, **43**, 131–136.
160 I. Lukovits, A. Shaban and E. Kálmán, *Russ. J. Electrochem.*, 2003, **39**, 177–181.
161 G. Tian and K. Yuan, *J. Mol. Model.*, 2021, **27**, 195.
162 E. E. Ebenso, M. M. Kabanda, L. C. Murulana, A. K. Singh and S. K. Shukla, *Ind. Eng. Chem. Res.*, 2012, **51**, 12940–12958.
163 L. C. Murulana, A. K. Singh, S. K. Shukla, M. M. Kabanda and E. E. Ebenso, *Ind. Eng. Chem. Res.*, 2012, **51**, 13282–13299.
164 S. Yesudass, L. O. Olasunkanmi, I. Bahadur, M. M. Kabanda, I. B. Obot and E. E. Ebenso, *J. Taiwan Inst. Chem. Eng.*, 2016, **64**, 252–268.
165 M.-F. Chen, Y. Chen, Z. Jia Lim and M. Wah Wong, *J. Mol. Liq.*, 2022, **367**, 120489.
166 T. W. Quadri, L. O. Olasunkanmi, O. E. Fayemi, E. D. Akpan, H.-S. Lee, H. Lgaz, C. Verma, L. Guo, S. Kaya and E. E. Ebenso, *Comput. Mater. Sci.*, 2022, **214**, 111753.
167 C. Verma, S. H. Alrefaee, M. A. Quraishi, E. E. Ebenso and C. M. Hussain, *J. Mol. Liq.*, 2021, **321**, 114484.
168 M. A. Deyab, M. T. Zaky and M. I. Nessim, *J. Mol. Liq.*, 2017, **229**, 396–404.
169 M. F. Shehata, A. M. El-Shamy, K. M. Zohdy, E.-S. M. Sherif and S. Zein El Abedin, *Appl. Sci.*, 2020, **10**, 1444.
170 W. Xiang, C. Zhao, C. Zhang, X. Wang, X. Li, S. Liu, C. Sun, Q. Yu, B. Yu, M. Cai and L. Shi, *Langmuir*, 2024, **40**(1), 389–402.
171 N. V. Likhanova, M. A. Domínguez-Aguilar, O. Olivares-Xometl, N. Nava-Entzana, E. Arce and H. Dorantes, *Corros. Sci.*, 2010, **52**, 2088–2097.
172 N. V. Likhanova, N. López-Prados, D. Guzmán-Lucero, O. Olivares-Xometl, I. V. Lijanova, P. Arellanes-Lozada and J. Arriola-Morales, *J. Adhes. Sci. Technol.*, 2022, **36**, 845–874.
173 O. Olivares-Xometl, I. V. Lijanova, N. V. Likhanova, P. Arellanes-Lozada, H. Hernández-Cocoletzi and J. Arriola-Morales, *J. Mol. Liq.*, 2020, **318**, 114075.
174 P. Arellanes-Lozada, V. Díaz-Jiménez, H. Hernández-Cocoletzi, N. Nava, O. Olivares-Xometl and N. V. Likhanova, *Corros. Sci.*, 2020, **175**, 108888.
175 S. Gurjar, S. K. Sharma, A. Sharma and S. Ratnani, *Electrochem. Sci. Adv.*, 2022, **2**, e2100110.